

# Phase-space representation of Landau and electron coherent states for uniaxially strained graphene

E Díaz-Bautista<sup>\*1,2</sup> and Y Betancur-Ocampo<sup>†3</sup>

<sup>1</sup>Departamento de Formación Básica Disciplinaria, Unidad Profesional Interdisciplinaria de Ingeniería Campus Hidalgo del Instituto Politécnico Nacional, Pachuca: Ciudad del Conocimiento y la Cultura, Carretera Pachuca-Actopan km 1+500, San Agustín Tlaxiaca, 42162 Hidalgo, México

<sup>2</sup>Departamento de Física, Cinvestav, P.O. Box. 14-740, 07000 Ciudad de México, México

<sup>3</sup>Instituto de Ciencias Físicas, Universidad Nacional Autónoma de México, 62210 Cuernavaca, México

## Abstract

Recent experimental advances in the reconstruction of the Wigner function (WF) in electronic systems have led us to consider the possibility of employing this theoretical tool in the analysis of electron dynamics of uniaxially strained graphene. In this work, we study the effect of strain on the WF of electrons in graphene under the interaction of a uniform magnetic field. This mechanical deformation modifies drastically the shape of the Wigner and Husimi function of Landau and coherent states. The WF has a different behavior straining the material along the zigzag direction in comparison with the armchair one and favors the obtention of electron coherent states. The time evolution of the WF for electron coherent states shows fluctuations between classical and quantum behavior with a local maximum value moving in a closed path. The phase-space representation shows more clearly the effect of non-equidistant of relative Landau levels in the time evolution of electron coherent states than other approaches. Our findings may be useful in establishing protocols for the realization of electron coherent states in graphene as well as a bridge between condensed matter and quantum optics.

## 1 Introduction

Quantum systems are traditionally described by using a probabilistic interpretation about them. From this notion the so-called wave function  $\psi$  arises, with which we can calculate the probability of finding a particle in some space region by taking its square norm  $|\psi|^2$ , or the probability

---

<sup>\*</sup>ediazba@ipn.mx; ediaz@fis.cinvestav.mx

<sup>†</sup>ybetancur@icf.unam.mx

that a certain system is in one state or another. Applying the so-called evolution operator, we can know how the probabilities change over time [1]. However, this formulation about how to quantize a system is not unique mainly because many physicist try to explain the apparent controversy between the superposition principle of quantum mechanics and the probabilistic results of measurement. As consequence, there are a variety of formulations of quantum mechanics that are based on different interpretations about the physical reality. Among such formulations, there is the phase-space representation which places the position and momentum variables on equal footing [2–10]. In this formulation of quantum mechanics, one leaves the wave function idea to adopt the quasiprobability distribution and the operator action is replaced by a star product [9]. Nowadays, Wigner function (WF) has been one of the most important theoretical tools for describing quantum systems in the phase-space representation [8]. This function has been widely used in different physics and chemistry branches [8]. Its most relevant role can be found in quantum physics, where it was possible to obtain an experimental reconstruction in quantum tomography experiments [11–16]. Since interference phenomena is more clearly understood due to that it is easier to recognize the pure states and their interacting parts. For that reason, WF is frequently used as a powerful tool for studying quantum information processes [17–19]. Recently, there is a significant increment in the employment of WF for electronic systems [20–27]. For instance, it has been used for the study of electron transport [21, 23, 27]. These different works have achieved to demonstrate that this quantum mechanics formulation allows a clear connection among different physics areas, by the simple reason that this representation treats electrons and photons indistinctly due to their wave nature. Likewise, interesting analogies between effective Dirac-like approach depicting of low energy excitations in graphene and Jaynes-Cummings model in quantum optics have been pointed out [28–34].

On the other hand, the emergence of strain-engineering has opened an important platform for exploiting the outstanding electronic, transport, and optical properties in graphene [35–80]. This topic started with the possibility of obtaining a gap opening [35, 38, 70], but later multiple interesting effects were predicted such as the generation of pseudo magnetic fields [60, 61, 65] through the application of inhomogeneous strain [60–67], the modulation of physical properties without detriment of the Dirac cones in a wide deformation range, giving rise for instance to the contraction of Landau levels (LLs) [49], optical absorption [37, 55, 59] and magnetostrain-driven quantum heat engines [81]. In this context, it also was predicted the realization of exotic ballistic transport phenomena as the collimation effect of electrons [36], valley beam splitters [44–48], Klein tunneling deviation and asymmetric Veselago lenses [50]. These inspiration works motivate us to introduce the Wigner matrix (WM) formalism for uniaxially strained graphene under the presence of a uniform magnetic field, in order to describe the electron dynamics in the phase-space representation. The recent advances about the quantum tomography of an electron [24] might stimulate to the experimental reconstruction of the WF in two-dimensional materials, particularly for uniaxially strained graphene due to the existing important experimental contributions so far [73–77]. Moreover, the resemblance of electron and light quantum optics is more evidenced from the WF analysis.

For these motivations, we propose the study of quasi-probability distributions for describing the time evolution of electron dynamics in uniaxially strained graphene under a uniform and perpendicular magnetic field. We start developing an effective Weyl-Dirac model based

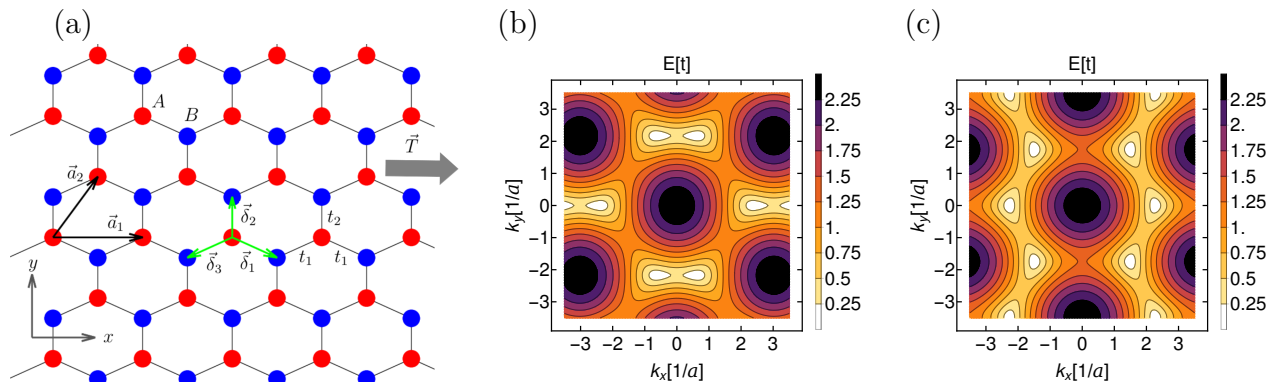


Figure 1: (a) Schematic representation of uniaxially strained graphene where red and blue circles indicate the sites of triangular sublattices A and B, respectively. Uniaxial strain along the zigzag or armchair direction has two different nearest neighbor hopping parameters  $t_1$  and  $t_2$ . The lattice vectors are denoted by  $\vec{a}_1$  and  $\vec{a}_2$ . (b) and (c) Energy contour of the conduction band near the first Brillouin zone for a deformation of 20% along the zigzag and armchair direction, respectively.

on Tight-Binding (TB) approach to nearest neighbors around a Dirac point. We relate the geometrical parameters of the elliptical Dirac cones with the components of the strain tensor showing a good agreement with recent Density Functional Theory (DFT) calculations [49]. Such parameters allow us to modulate successfully the shape of the WF through the tensile parameter. We calculate the Landau states from our effective model. Using the integral representation of the WF, we determine the components of the WM as a function of the tensile strain and the magnitude of magnetic field. We also build electron coherent states from the Landau quantization through the eigenstates of annihilation operators of pseudo-spin 1/2 systems and obtain the corresponding WM. We find that stretching along the zigzag ( $\mathcal{Z}$ ) direction favors the obtention of electron coherent states. From the time evolution of the WM of electron coherent states, we identify aspects of electron classical motion in a uniform magnetic field as well as the evidence of fluctuations in the quasi-probability distribution, where negative values indicate a non-classical behavior of these states. At the time this work has been developed, the analysis of time evolution of electron dynamics in phase-space for strained two-dimensional materials has not yet been performed.

## 2 Effective Tight-Binding Hamiltonian in uniaxially strained graphene

### 2.1 Tight-Binding approach to nearest neighbors

For describing adequately the WM in deformed graphene, we start using the TB approach to an anisotropic hexagonal lattice [35, 50, 53, 79]. In this approach, the  $p_z$  orbital of the carbon atom is decoupled with the  $\sigma$  ones. Other approximations are also taken into account such as

the neglecting of overlap between  $p_z$  orbitals and second nearest neighbor interactions. Since there are two atoms per unit cell and we assume an infinity extended layer, the TB is simplified considerably and reduced to a model of two energy bands [50, 82, 83]. This effective model only depends of two hopping parameters  $t_1$  and  $t_2$  for quinoid type deformations which quantify the probability amplitude that an electron hops to the nearest atom. The main properties of strained graphene depend strongly of the value of these parameters. For instance an excessive value of one of them can cause a gap opening [35, 38]. These parameters are related directly with the bond lengths. Thus, when a uniaxial tension  $T$  is applied to graphene, the atomic sites are displaced and modify the hopping parameter values, as shown in Fig. 1. The positions of nearest neighbors are denoted by  $\vec{\delta}_1$ ,  $\vec{\delta}_2$  and  $\vec{\delta}_3$  on the underlying sublattice A, where the Cartesian system is set with the  $x$ -axis along the  $\mathcal{Z}$  bond. The lattice vectors  $\vec{a}_1$  and  $\vec{a}_2$  allow connect the whole positions in the deformed hexagonal lattice. From elasticity theory [35, 40, 41, 84], the uniaxial strain tensors along  $\mathcal{Z}$  and armchair ( $\mathcal{A}$ ) directions are written respectively as

$$\epsilon_{\mathcal{Z}} = \begin{pmatrix} 1 & 0 \\ 0 & -\nu \end{pmatrix} \epsilon, \quad \epsilon_{\mathcal{A}} = \begin{pmatrix} -\nu & 0 \\ 0 & 1 \end{pmatrix} \epsilon \quad (1)$$

where  $\nu$  is the Poisson ratio of graphene [36, 40] and the tensile strain  $\epsilon$  is proportional to the magnitude of tension  $T$ , namely, it quantifies the percentage of deformation [35]. According to Eq. (1), when a positive (negative) deformation  $\epsilon$  is applied along a particular axis, the perpendicular direction is contracted (expanded) by a quantity of  $-\nu\epsilon$ . The atomic positions in uniaxially strained graphene are given by  $\vec{r} = (\mathbb{I} + \bar{\epsilon})\vec{r}_0$ , where  $\vec{r}_0$  indicates the sites on the pristine graphene,  $\mathbb{I}$  denotes the  $2 \times 2$  unity matrix and  $\bar{\epsilon}$  is the deformation tensor. Thus, the deformed lattice vectors for uniaxial strain in  $\mathcal{Z}$  direction are

$$\vec{a}_1^{\mathcal{Z}} = \sqrt{3}a_0\hat{x}(1 + \epsilon), \quad (2a)$$

$$\vec{a}_2^{\mathcal{Z}} = \frac{\sqrt{3}}{2}a_0[\hat{x}(1 + \epsilon) + \sqrt{3}\hat{y}(1 - \nu\epsilon)], \quad (2b)$$

while the  $\mathcal{A}$  direction they are

$$\vec{a}_1^{\mathcal{A}} = \sqrt{3}a_0\hat{x}(1 - \nu\epsilon), \quad (3a)$$

$$\vec{a}_2^{\mathcal{A}} = \frac{\sqrt{3}}{2}a_0[\hat{x}(1 - \nu\epsilon) + \sqrt{3}\hat{y}(1 + \epsilon)], \quad (3b)$$

where  $a_0$  is the bond length in pristine graphene [42]. Since the nearest neighbor sites are given by  $\vec{\delta}_1 = 2\vec{a}_1/3 - \vec{a}_2/3$ ,  $\vec{\delta}_2 = 2\vec{a}_2/3 - \vec{a}_1/3$ , and  $\vec{\delta}_3 = -\vec{\delta}_1 - \vec{\delta}_2$ , they are also related with the tensile strain.

In order to obtain an effective model based on the TB approach, we develop the following TB Hamiltonian in the Fourier basis from a plane wave *ansatz* [50, 82]

$$H_{\text{TB}}^K = \sum_{j=1}^3 \begin{bmatrix} 0 & t_j e^{i\vec{k} \cdot \vec{\delta}_j} \\ t_j e^{-i\vec{k} \cdot \vec{\delta}_j} & 0 \end{bmatrix}. \quad (4)$$

The hopping parameters  $t_j$  can be modeled using an exponential decay rule  $t_j = t \exp[-\beta(\delta_j/a - 1)]$ , where  $\beta$  is the Grüneisen constant,  $t$  is the hopping in pristine graphene, and  $\delta_j$  are the



deformed bond lengths [35, 42, 50, 85]. The relation of  $t_j$  as a function of strain parameters is completed when we express the deformed lengths in terms of tensile strain, which for  $\mathcal{Z}$  deformations are given by

$$\delta_1^{\mathcal{Z}} = \delta_3^{\mathcal{Z}} = a_0 \sqrt{\left[1 + \frac{1}{4}(3 - \nu)\epsilon\right]^2 + \frac{3}{16}(1 + \nu)^2\epsilon^2}, \quad (5a)$$

$$\delta_2^{\mathcal{Z}} = a_0(1 - \nu\epsilon), \quad (5b)$$

while for uniaxial strain along the  $\mathcal{A}$  direction

$$\delta_1^{\mathcal{A}} = \delta_3^{\mathcal{A}} = a_0 \sqrt{\left[1 + \frac{1}{4}(1 - 3\nu)\epsilon\right]^2 + \frac{3}{16}(1 + \nu)^2\epsilon^2}, \quad (6a)$$

$$\delta_2^{\mathcal{A}} = a_0(1 + \epsilon). \quad (6b)$$

The electronic band structure of uniaxially strained graphene is obtained from the eigenenergies of the Hamiltonian (4)

$$E_s(\vec{k}) = s \left| \sum_{j=1}^3 t_j e^{-i\vec{k} \cdot \vec{\delta}_j} \right|, \quad (7)$$

where the band index  $s = 1(-1)$  corresponds to the conduction (valence band). The energy bands can be modified applying uniaxial strain, as shown in Fig. 1(b) and (c). DFT and TB calculations have an excellent agreement within low energy regime [39]. For that reason, the TB Hamiltonian (4) is expanded around the Dirac point performing  $\vec{k} = \vec{q} + \vec{K}_D$  and the Dirac point position  $\vec{K}_D$  satisfies  $\sum_j t_j \exp(-i\vec{K}_D \cdot \vec{\delta}_j) = 0$ . Thus, the effective Dirac-Weyl-like Hamiltonian in the continuum approximation is

$$H_D = v_F \begin{bmatrix} 0 & ap_x - ibp_y \\ ap_x + ibp_y & 0 \end{bmatrix}, \quad (8)$$

where the quantities

$$a = \frac{2}{3} \sum_{j=1}^3 \frac{\delta_{jx} t_j}{a_0 t} \sin(\vec{K}_D \cdot \vec{\delta}_j), \quad (9a)$$

$$b = \frac{2}{3} \sum_{j=1}^3 \frac{\delta_{jy} t_j}{a_0 t} \cos(\vec{K}_D \cdot \vec{\delta}_j). \quad (9b)$$

are expressed as functions of the lattice vectors and hopping parameters. Taking into account the relation

$$\cos[\vec{K}_D \cdot (\vec{\delta}_1 - \vec{\delta}_2)] = -\frac{t_2}{2t_1}, \quad (10)$$

which is obtained from the Dirac points equation  $\sum_j^3 t_j e^{-i\vec{K}_D \cdot \vec{\delta}_j} = 0$ , it is possible to show that

$$\begin{aligned} a &= \frac{2}{3a_0 t} \sqrt{a_{1x}^2 t_1^2 + (a_{2x} - a_{1x})a_{2x} t_2^2}, \\ b &= \frac{2}{3a_0 t} \sqrt{a_{1y}^2 t_1^2 + (a_{2y} - a_{1y})a_{2y} t_2^2}. \end{aligned} \quad (11)$$

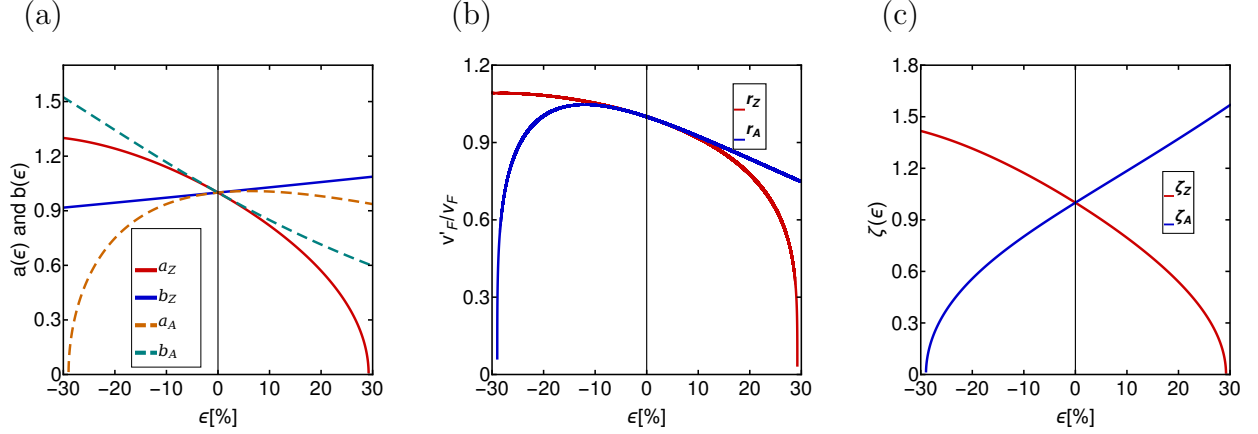


Figure 2: Geometrical parameters  $a$  and  $b$  (a), effective Fermi velocity  $v_F' = v_F\sqrt{ab}$  (b), and supersymmetric potential parameter  $\zeta = a/b$  (c) as a function of the tensile strain parameter  $\epsilon$  along the zigzag and armchair directions.

It is important to mention that the parameters  $a$  and  $b$  can be related with the extremal angle of the elliptical Dirac cones [49]. This shows clearly that the physical properties of strained graphene can be modulated by the geometrical parameters of the Dirac cone and therefore of the strain using the relation (11). These quantities depend on the strain direction by evaluating the corresponding expressions of lattice vectors (2) and (3) and bond lengths (5) and (6) for  $\mathcal{Z}$  and  $\mathcal{A}$  directions. In the geometrical approach, the parameters  $a$  and  $b$  are fitted to the energy bands obtained from DFT calculations [49]. The behavior of  $a$  and  $b$  given by Eq. (11) as a function of strain is similar to the observed from the geometrical approach [49], see Fig. 2(a). We can observe that for strain values up to 10% the geometrical parameters satisfies  $a_Z \approx b_A$  and  $b_Z \approx a_A$ . Beyond this range, these geometrical parameters are different. This behavior is in accordance with the stress-strain relationship of graphene [40], the elastic response is isotropic and linear for  $\epsilon < 10\%$  while it is nonlinear and anisotropic for  $\epsilon > 10\%$ . Therefore, the analytical formulae (11) indicates adequately how the strain affects the geometrical parameters  $a$  and  $b$  and other electronic properties such as effective Fermi velocity  $v_F' = v_F\sqrt{ab}$  (see Fig. 2(b)), the supersymmetric potential parameter  $\zeta = a/b$  (see Fig. 2(c)), and as we will show in forthcoming sections the WF of Landau and coherent states.

## 2.2 Dirac-Weyl equation under uniaxial strain

The effective Dirac-Weyl Hamiltonian (8) has validity in the energy range of 0-0.3 eV, where DFT and TB calculations perfectly agree [39]. It is important to mention that exist other models for depicting electronic properties of strained graphene using a pseudo-vector potential. Such theoretical works have been useful for studying graphene under inhomogeneous deformations [52]. However, in the uniform strain case has been shown that such models do not describe correctly the electron dynamics because the high symmetry point  $K$  in the first Brillouin zone is far away from the Dirac point, where dispersion relation can be nonlinear [53]. For that

reason, an effective Dirac-Weyl model around the Dirac point is more adequate for studying the physical properties of uniaxially strained graphene instead of one in the high symmetry points. Moreover, this model constitutes a simple way to promote the Fermi velocity to a tensor character and that prevents the generation of pseudomagnetic fields due to the homogeneity of the deformation. An analogous procedure can be implemented at the  $K'_D$  valley to obtain the corresponding effective Dirac-like Hamiltonian.

Now, let us consider the Dirac-Weyl (DW) equation under uniform uniaxial strain

$$H\Psi(x, y) = v_F(a\sigma_x\pi_x + b\sigma_y\pi_y)\Psi(x, y) = E\Psi(x, y), \quad (12)$$

where the geometrical parameters  $a, b$  are given by Eq. (11), the linear momentum in presence of a magnetic field and under the Peierls substitution is  $\pi_{x,y} = p_{x,y} + eA_{x,y}$ , with  $\vec{p}$  being the kinetic momentum in free-field and  $\vec{A}$  the vector potential that generates a magnetic field aligned perpendicularly to the graphene sample. In a Landau-like gauge,

$$\vec{A}(x, y) = A_y(x)\hat{y}, \quad \vec{B} = \nabla \times \vec{A} = B(x)\hat{z}, \quad (13)$$

the linear momentum  $p_y = \hbar k$ , with  $k$  the wave vector in  $y$ , is conserved and therefore we can write the pseudo-spinor *ansatz* as

$$\Psi(x, y) = \exp(iky) \begin{pmatrix} \psi^+(x) \\ \psi^-(x) \end{pmatrix}. \quad (14)$$

Substituting (14) into (12), two coupled equations arise, namely

$$[ap_x \pm ib(k\hbar + eA_y(x))] \psi^\pm(x) = \frac{E}{v_F} \psi^\mp(x). \quad (15)$$

These equations are decoupled to obtain

$$\left[ -\zeta \frac{d^2}{dx^2} + V_\zeta^\pm(x) \right] \psi^\pm(x) = \varepsilon^{\pm 2} \psi^\pm(x), \quad (16)$$

where  $\varepsilon^\pm = E/(v_F\hbar\sqrt{ab})$  and

$$V_\zeta^\pm(x) = \zeta^{-1} \left( k + \frac{eA_y(x)}{\hbar} \right)^2 \pm \frac{e}{\hbar} \frac{dA_y(x)}{dx}. \quad (17)$$

This effective one-dimensional potential has been discussed in a supersymmetric point of view [86] and we show how this potential through the parameter  $\zeta$  is tuned with the tensile strain  $\epsilon$  in Fig. 2(c). In the case of inhomogenous magnetic field, there is a little number of vector potential profiles that allow to obtain exact and analytical solutions of energy level spectra and wave functions of the electron [86, 87], but in general, it is necessary to solve numerically the Sturm-Liouville problem given by the decoupled systems (16). For a uniform magnetic field  $\vec{B} = B\hat{z}$  we can obtain an exact solution using the Landau gauge  $\vec{A} = Bx\hat{y}$ . In this way, the Hamiltonians and effective potential in the supersymmetric approach are, respectively,

$$H_\zeta^\pm = -\zeta \frac{d^2}{dx^2} + V_\zeta^\pm(x), \quad V_\zeta^\pm(x) = \frac{\zeta\omega_\zeta^2}{4} \left( x + \frac{2k}{\zeta\omega_\zeta} \right)^2 \pm \frac{\zeta\omega_\zeta}{2}, \quad (18)$$

where  $\omega_\zeta$  is a frequency defined by  $\omega_\zeta = \frac{2eB}{\hbar}$ . Since this problem is very similar to solve the quantum harmonic oscillator, the LLs spectra is straightforwardly obtained [49]

$$E_n = sv'_F \sqrt{2ne\hbar B}, \quad (19)$$

where  $v'_F = v_F \sqrt{ab}$  is the effective Fermi velocity. The Landau level index  $n$  runs over  $0, 1, 2, \dots$  and the positive (negative) energy corresponds to electrons in the conduction (valence) band, as given by the band index  $s$ . When one performs the same analysis in the other elliptical Dirac cone  $K'_D$ , the LLs spectra is very similar to the shown in (19). However, each valley contributes in a different way for the Landau state with  $n = 0$  [82], namely, the zeroth Landau state receives a contribution of the sublattice A (B) in the valley  $K_D$  ( $K'_D$ ). This important fact gives rise to the anomalous quantum Hall effect [88–90]. Furthermore, the quantity  $\sqrt{ab}$  is always less than one for positive deformations, (see Fig. 2(b)), causing the contraction of LLs spectra [49, 91]. In contrast, for compressing graphene lattice the quantity  $\sqrt{ab}$  increases and we can expand the LLs spectra. It is important to mention that the LLs in Eq. (19) are only valid for low magnetic fields and energies [82, 83]. Such an observation is useful if one considers to build electron coherent states in uniaxially strained graphene, since the major possible number of LLs are needed within the energy range where the dispersion relation is linear. In this way, the most convenient route for a tentative obtention of electron coherent states is stretching graphene along the  $\mathcal{Z}$  direction and using low magnetic fields. As seen in Fig. 2(b), the Fermi velocity is lower in  $\mathcal{Z}$  than  $\mathcal{A}$  direction for positive deformations and therefore the LLs spectra is compressed more efficiently.

The exact solution for the wave function of electrons in strained graphene with a uniform magnetic field turns out to be

$$\Psi_n(x, y) = \frac{\exp(iky)}{\sqrt{2^{(1-\delta_{0n})}}} \begin{pmatrix} (1 - \delta_{0n})\psi_{n-1}(x) \\ i\lambda s \psi_n(x) \end{pmatrix}, \quad (20)$$

and the components of the pseudo-spinor are given by

$$\psi_n(x) = \sqrt{\frac{1}{2^n n!} \left(\frac{\omega_\zeta}{2\pi}\right)^{1/2}} \exp\left[-\frac{\omega_\zeta}{4} \left(x + \frac{2k}{\zeta\omega_\zeta}\right)^2\right] H_n\left[\sqrt{\frac{\omega_\zeta}{2}} \left(x + \frac{2k}{\zeta\omega_\zeta}\right)\right]. \quad (21)$$

The quantity  $\delta_{mn}$  denotes the Kronecker delta,  $\psi_n^- \equiv \psi_n$ ,  $\psi_n^+ \equiv \psi_{n-1}$  and  $\lambda = +/-$  describes Dirac fermions at the  $K_D/K'_D$  valley. It is worth to remark that the wave function in the upper (lower) component of the pseudo-spinor (20) corresponds to an electron at the  $K_D$  valley in the sublattice A (B), while at the  $K'_D$  valley the role of upper and lower components are interchanged. These wave functions will be used for determining the coherent states and WM from an integral representation. In all our calculations, we set the following physical constants  $\hbar = e = 1$ . Besides, without loss of generality, in the next sections we will focus on the conduction band ( $s = 1$ ).

### 3 Electron coherent states of strained graphene

#### 3.1 Annihilation operator

For obtaining coherent states in electronic systems first we introduce the definition of creation and annihilation operators for electrons of strained graphene in presence of a uniform magnetic field. Thus, let us define the following dimensionless differential operators

$$\theta^\pm = \frac{1}{\sqrt{2}} \left( \mp \frac{d}{d\xi} + \xi \right), \quad \theta^+ = (\theta^-)^\dagger, \quad \xi = \sqrt{\frac{\omega_\zeta}{2}} \left( x + \frac{2k}{\zeta\omega_\zeta} \right), \quad (22)$$

that satisfy the commutation relation

$$[\theta^-, \theta^+] = 1. \quad (23)$$

This relation implies that the set of operators  $\{\theta^+, \theta^-, 1\}$  generate a Heisenberg-Weyl (HW) algebra [92–94].

Now, the action of the operators  $\theta^\pm$  on the eigenfunctions  $\psi_n$  in (21) is

$$\theta^- \psi_n = \sqrt{n} \psi_{n-1}, \quad \theta^+ \psi_n = \sqrt{n+1} \psi_{n+1}, \quad (24)$$

so that  $\theta^-$  ( $\theta^+$ ) is the annihilation (creation) operator. In terms of these ladder operators, we can define the following dimensionless  $2 \times 2$  Hamiltonian  $\mathcal{H}$  that acts on the  $x$ -dependent pseudo-spinors in Eq. (20)

$$\mathcal{H} = \begin{bmatrix} 0 & -i\theta^- \\ i\theta^+ & 0 \end{bmatrix}. \quad (25)$$

In order to build coherent states in graphene, one can define a generalized annihilation operator  $\Theta^-$  as

$$\Theta^- = \begin{bmatrix} \cos(\delta) \frac{\sqrt{N+2}}{\sqrt{N+1}} \theta^- & \lambda \sin(\delta) \frac{1}{\sqrt{N+1}} (\theta^-)^2 \\ -\lambda \sin(\delta) \sqrt{N+1} & \cos(\delta) \theta^- \end{bmatrix}, \quad \Theta^+ = (\Theta^-)^\dagger, \quad (26)$$

such that

$$\Theta^- \Psi_n(x, y) = \frac{\exp(i\delta)}{\sqrt{2^{\delta_{1n}}}} \sqrt{n} \Psi_{n-1}(x, y), \quad n = 0, 1, 2, \dots, \quad (27)$$

where  $N = \theta^+ \theta^-$  is the number operator. The parameter  $\delta \in [0, 2\pi]$  in Eq. (26) allows us to consider either a diagonal or non-diagonal form for such operator in order to mix, exchange or not the components that belong to different sublattices (A or B) in the pseudo-spinor.

On the other hand, the operators  $\Theta^\pm$  satisfy the following commutation relation

$$[\Theta^-, \Theta^+] = \mathbb{I}, \quad (28)$$

that also generates a HW algebra.

### 3.2 Coherent states as eigenstates of $\Theta^-$

We obtain the coherent states  $\Psi_\alpha(x, y)$  as eigenstates of the operator  $\Theta^-$ :

$$\Theta^- \Psi_\alpha(x, y) = \alpha \Psi_\alpha(x, y), \quad \alpha \in \mathbb{C}, \quad (29)$$

where  $\alpha$  is the eigenvalue of  $\Theta^-$ . The  $|\alpha|^2$  indicates the average electron number, while the  $\alpha$  phase is the polar angle in phase-space. The electron coherent states are expanded in the Landau states basis (21) as

$$\Psi_\alpha(x, y) = a_0 \Psi_0(x, y) + \sum_{n=1}^{\infty} a_n \Psi_n(x, y). \quad (30)$$

Upon inserting these states into the corresponding eigenvalue equation, we get the following relations

$$a_1 = \sqrt{2} \tilde{\alpha} a_0, \quad a_{n+1} \sqrt{n+1} = \tilde{\alpha} a_n, \quad (31)$$

where  $\tilde{\alpha} = \alpha \exp(-i\delta)$ . This means that the  $\delta$ -parameter translates as a phase factor that will affect the eigenvalue  $\alpha$  and  $a_0$  is a free parameter that can be determined by the normalization process.

After straightforward calculations, the coherent states turn out to be [93]:

$$\begin{aligned} \Psi_\alpha(x, y) &= \frac{1}{\sqrt{2 \exp(|\tilde{\alpha}|^2) - 1}} \left[ \Psi_0(x, y) + \sum_{n=1}^{\infty} \frac{\sqrt{2} \tilde{\alpha}^n}{\sqrt{n!}} \Psi_n(x, y) \right] \\ &= \frac{e^{iky}}{\sqrt{2 \exp(|\tilde{\alpha}|^2) - 1}} \begin{pmatrix} \psi'_\alpha(x) \\ i\psi_\alpha(x) \end{pmatrix}, \end{aligned} \quad (32)$$

where

$$\psi'_\alpha(x) = \left( \frac{\omega_\zeta}{2\pi} \right)^{1/4} \exp\left(-\frac{\xi^2}{2}\right) \sum_{n=1}^{\infty} \frac{(\tilde{\alpha}/\sqrt{2})^n}{n!} \sqrt{2n} H_{n-1}(\xi), \quad (33a)$$

$$\psi_\alpha(x) = \left( \frac{\omega_\zeta}{2\pi} \right)^{1/4} \exp\left(-\frac{\xi^2}{2} - \frac{\tilde{\alpha}^2}{2} + \sqrt{2} \tilde{\alpha} \xi\right). \quad (33b)$$

Eq. (33b) corresponds to the wave function of an unnormalized standard coherent state.

## 4 Phase-space representation

### 4.1 Properties of Wigner and Husimi function in quantum mechanics

The Wigner function  $W(\vec{r}, \vec{p})$  is the cornerstone of quantum mechanics in phase-space. It is a quasiprobability distribution defined as [2–5]

$$W(\vec{r}, \vec{p}) = \frac{1}{(2\pi\hbar)^n} \int_{-\infty}^{\infty} \exp\left(\frac{i}{\hbar} \vec{p} \cdot \vec{r}'\right) \left\langle \vec{r} - \frac{\vec{r}'}{2} \left| \rho \right| \vec{r} + \frac{\vec{r}'}{2} \right\rangle d\vec{r}', \quad (34)$$

where  $\rho$  is the density matrix,  $\vec{r} = (r_1, r_2, \dots, r_n)$  and  $\vec{p} = (p_1, p_2, \dots, p_n)$  are  $n$ -dimensional vectors representing the classical phase-space position and momentum values, respectively, and  $\vec{r}' = (r'_1, r'_2, \dots, r'_n)$  is the position vector in the integration process. The normalization condition is given by

$$\int_{-\infty}^{\infty} \int_{-\infty}^{\infty} W(\vec{r}, \vec{p}) d\vec{r} d\vec{p} = 1. \quad (35)$$

It is a real function that can take negative values, in contrast with the probability density of any quantum state. Such *negativity* has no physical meaning if it is thought like a probability distribution. In several works the negativity in WF has been considered as an indicator of the non-classicality of a state and being interpreted as a sign of *quantumness*. This feature has been tested experimentally [95–103]. However in 2D phase-space, for instance, the WF can be used for obtaining the  $x$  and  $p$  probability distributions

$$\int_{-\infty}^{\infty} W(x, p) dp = |\psi(x)|^2, \quad \int_{-\infty}^{\infty} W(x, p) dx = |\varphi(p)|^2. \quad (36)$$

#### 4.1.1 Husimi function

Other phase-space representation is given by the Husimi function. The Husimi  $Q$  representation is a quasiprobability distribution commonly used in quantum mechanics to represent the distribution of a quantum state in the phase-space formulation [6]. It is used in the field of quantum optics and particularly for tomographic purposes [104] and in the study of quantum effects in superconductors [105].

The  $Q$ -function is defined by the expression

$$Q(\alpha) = \frac{1}{\pi} \langle \alpha | \rho | \alpha \rangle, \quad (37)$$

*i.e.*, it is a trace of the density matrix  $\rho$  over the basis of coherent states  $\{|\alpha\rangle\}$ . Also, it satisfies the following relations

$$\int_{\mathbb{C}} Q(\alpha) d^2\alpha = 1, \quad 0 \leq Q(\alpha) \leq \frac{1}{\pi}. \quad (38)$$

Both Husimi and WF are related through the Weierstrass transformation [106]

$$Q(\alpha) = \frac{2}{\pi} \int_{\mathbb{C}} W(\beta) \exp(-2|\alpha - \beta|^2) d^2\beta. \quad (39)$$

As an example, for the standard coherent states (SCS) of the standard harmonic oscillator (SHO), and with  $\rho = |\beta\rangle\langle\beta|$ , the Husimi function is given by

$$Q(\alpha) = \frac{1}{\pi} |\langle \alpha | \beta \rangle|^2 = \frac{1}{\pi} \exp(-[|\alpha|^2 + |\beta|^2] + \alpha\beta^* + \alpha^*\beta). \quad (40)$$

Since the parameter  $\alpha$  of SCS minimizes the Heisenberg uncertainty principle, the projection of the distribution of probabilities in the phase space represented by the Husimi  $Q(\alpha)$  function is a disk that will conserve its shape along the trajectories in phase space.



#### 4.1.2 Wigner function for Landau states in uniaxially strained graphene

In order to calculate the Wigner matrix for the Landau state  $n$  in the valley  $K_D$ , we have to take into account that the  $n \neq 0$  level presents a four-fold degeneracy due to the pseudo-spin of sublattice and valley, while the ground state  $n = 0$  has only two-fold degeneracy [88, 89]. We perform our analysis in the  $K_D$  valley finding a  $2 \times 2$  WM when we substitute the  $n$ -th eigenstate in Eq. (20) into the Wigner representation (34):

$$W_n(\vec{r}, \vec{p}) = \frac{1}{2^{(1-\delta_{0n})}} W(y, p_y) \begin{pmatrix} (1 - \delta_{0n})W_{n-1,n-1}(x, p_x) & -i\lambda(1 - \delta_{0n})W_{n-1,n}(x, p_x) \\ i\lambda(1 - \delta_{0n})W_{n,n-1}(x, p_x) & W_{n,n}(x, p_x) \end{pmatrix}, \quad (41)$$

where the components  $W_{\alpha,\beta}(x, p_x)$  and  $W(y, p_y)$  are given respectively by

$$W_{\alpha,\beta}(x, p_x) = \frac{1}{\pi\hbar} \int_{-\infty}^{\infty} \exp\left(2\frac{i}{\hbar}p_x z_1\right) \psi_\alpha(x - z_1)\psi_\beta^*(x + z_1)dz_1, \quad (42a)$$

$$W(y, p_y) = \frac{1}{\pi\hbar} \int_{-\infty}^{\infty} \exp\left(2i\left(\frac{p_y}{\hbar} - k\right)z_2\right) dz_2 \equiv \delta(p_y - k\hbar). \quad (42b)$$

being  $\psi_\alpha$  and  $\psi_\beta$  the wave functions of the quantum harmonic oscillator (21).

In order to compute the function  $W_{\alpha,\beta}(x, p_x)$ , we define the following quantities

$$\xi = \sqrt{\frac{\omega_\zeta}{2}} \left(x + \frac{2k}{\zeta\omega_\zeta}\right), \quad y = \sqrt{\frac{\omega_\zeta}{2}} \frac{z_1}{\hbar}, \quad s = \sqrt{\frac{2}{\omega_\zeta}} p_x. \quad (43)$$

Hence, by substituting Eq. (21) in (42a) and using the definitions (43), we get

$$W_{\alpha,\beta}(\chi) = \frac{\exp(-\frac{1}{2}|\chi|^2)}{\pi} \times \begin{cases} (-1)^\alpha \sqrt{\frac{\alpha!}{\beta!}} \chi^{\beta-\alpha} L_\alpha^{\beta-\alpha}(|\chi|^2), & \text{if } \alpha \leq \beta, \\ (-1)^\beta \sqrt{\frac{\beta!}{\alpha!}} \chi^{*\alpha-\beta} L_\beta^{\alpha-\beta}(|\chi|^2), & \text{if } \alpha \geq \beta, \end{cases} \quad (44)$$

where  $L_n^m(x)$  are the associated Laguerre polynomials and the quantity  $\chi = \sqrt{2}(\xi + is)$  is defined. Thus, the components of the  $2 \times 2$  WM turn out to be

$$W_{n-1,n-1}(\chi) = \frac{1}{\pi} (-1)^{n-1} \exp\left(-\frac{1}{2}|\chi|^2\right) L_{n-1}(|\chi|^2), \quad (45a)$$

$$W_{n-1,n}(\chi) = W_{n,n-1}^*(\chi) = \frac{(-1)^{n-1}}{\pi\sqrt{n}} \chi \exp\left(-\frac{1}{2}|\chi|^2\right) L_{n-1}^1(|\chi|^2), \quad (45b)$$

$$W_{n,n}(\chi) = \frac{1}{\pi} (-1)^n \exp\left(-\frac{1}{2}|\chi|^2\right) L_n(|\chi|^2), \quad (45c)$$

An identical solution for the WM in Eq. (45) is found in Appendix A using the Moyal  $\star$ -product. In these components we can identify the quantity  $\mathcal{E} = \frac{1}{2}|\chi|^2 = \xi^2 + s^2$  or, more explicitly,

$$\mathcal{E} = \frac{2}{\omega_\zeta} p_x^2 + \frac{\omega_\zeta}{2} \left(x + \frac{2k}{\zeta\omega_\zeta}\right)^2 = \exp(2\tau) p_x^2 + \exp(-2\tau) \left(x + \frac{2k}{\zeta\omega_\zeta}\right)^2, \quad (46)$$

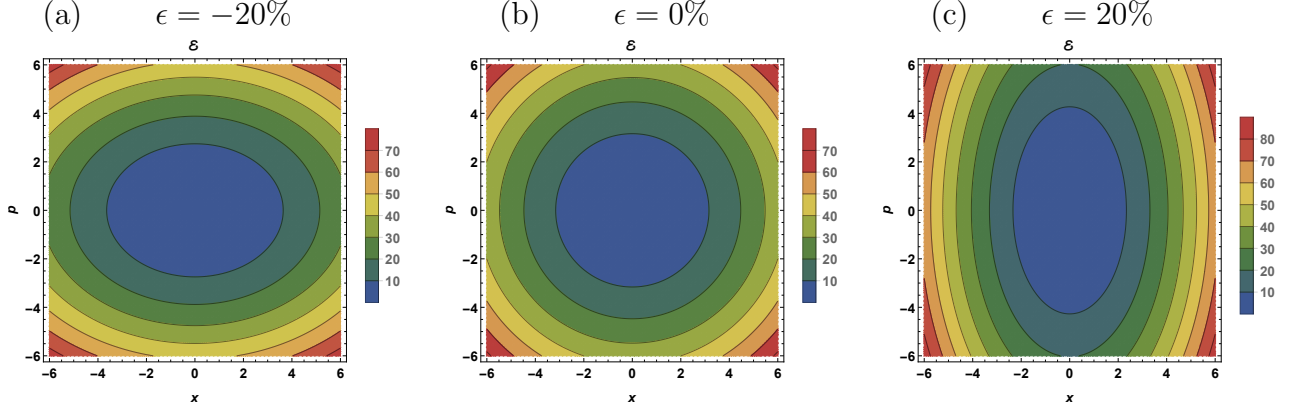


Figure 3: Qualitative behavior of the classical energy  $\mathcal{E}$  for different values of the tensile strain  $\epsilon$  along the zigzag direction. We set of the values  $B = 1$  and  $k = 0$ .

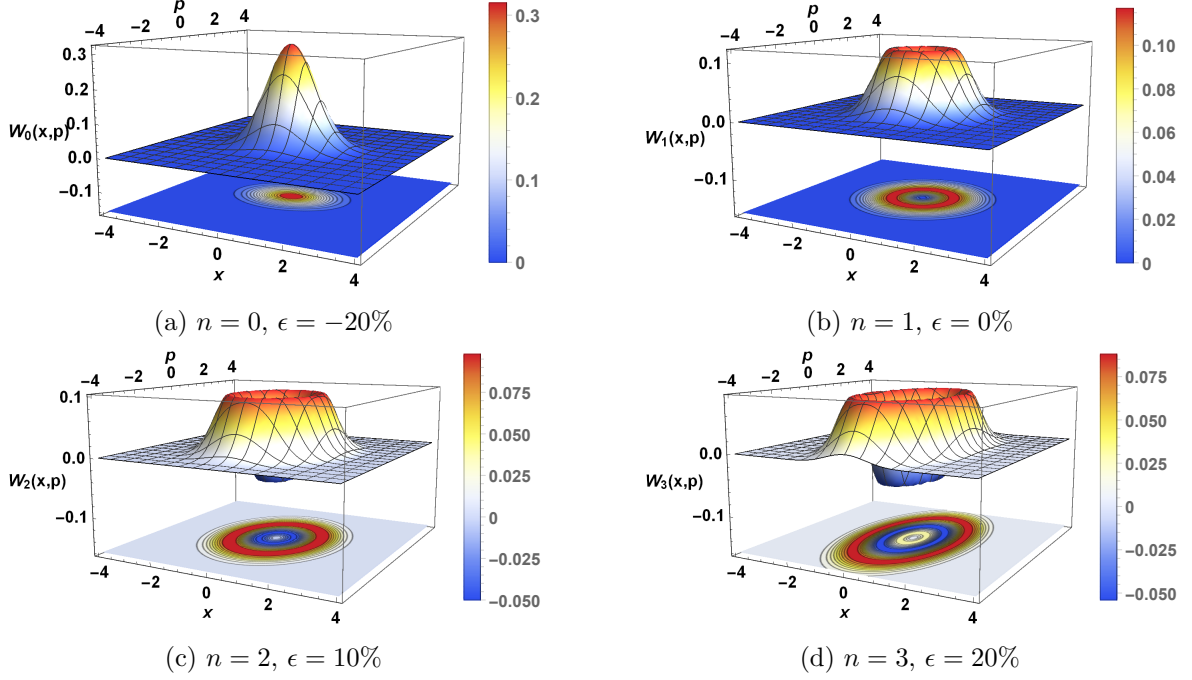


Figure 4: Trace of the Wigner matrix  $W_n(\vec{r}, \vec{p})$  in Eq. (41) for different values of  $n$  and  $\epsilon$  along the zigzag direction. In all these cases  $B = 1$  and  $k = 0$ .

where  $\tau = \ln \sqrt{2/\omega_\zeta}$ . Eq. (46) is the classical energy of a particle with linear momentum  $p_x$  moving in an oscillator potential whose center is depending on  $k$ . Such as occurs in classical mechanics,  $\mathcal{E}$  is represented by ellipses in phase-space. The effect of uniaxial strain is to change the length of semi-major axis according to the value of  $\epsilon$  through the amount  $\tau$  in Eq. (46), as shown in Fig. 3. This fact is recognizable in the WF for the Landau states of uniaxially strained graphene.

The elements of  $W(\vec{r}, \vec{p})$  also have a direct physical interpretation. As seen in wave function

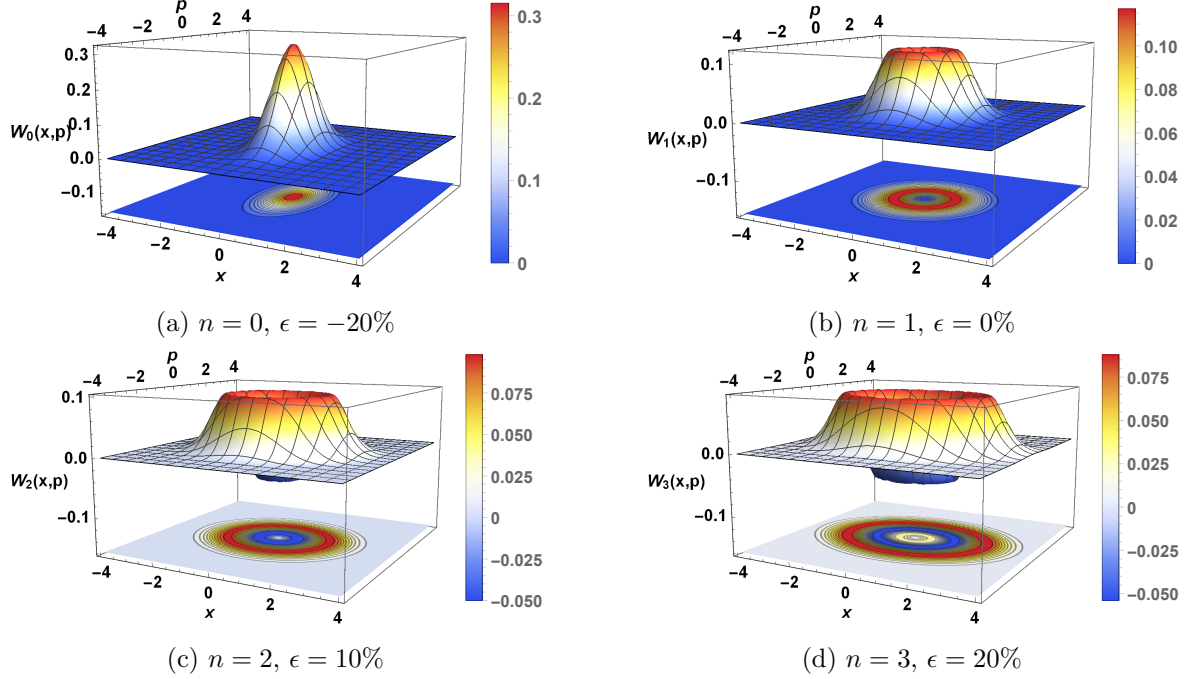


Figure 5: Trace of the Wigner matrix  $W_n(\vec{r}, \vec{p})$  in Eq. (41) for different values of  $n$  and  $\epsilon$  along the armchair direction. In all these cases  $B = 1$  and  $k = 0$ .

(20) the electron in sublattice A (B) has a quantum harmonic-like oscillator wave function  $(1 - \delta_{n0})\psi_{n-1}$  ( $\psi_n$ ). Therefore,  $W_{nn}$  and  $W_{n-1n-1}$  are the WFs for the electrons belong to the sublattice A and B, respectively with energy  $E_n$ . Meanwhile  $W_{n-1,n}$  can be recognized as the mixed WF for an electron in the sublattices A and B. This term can be very important for the case where  $e-e$  interaction is considered in order to describe interference phenomena. However, our analysis is restricted for a single particle model. Therefore, we only address the diagonal terms in the WM. Moreover, due to that one can choose an adequate representation in which WM is diagonal [107], we will just focus in analyzing the trace of matrix  $W_n(\vec{r}, \vec{p})$  in (41) that is an invariant quantity.

Figures 4 and 5 show that the surface of Wigner is distorted in a different way for deformations along the  $\mathcal{Z}$  and  $\mathcal{A}$  directions with strain values close to 20%. This evidences that the WF changes in accordance with the stress-strain relationship of graphene [40, 41], where anisotropic and nonlinear elastic behavior are obtained for strains up to 29%, as shown in Figs. 4(d) and 5(d) for the particular case  $n = 3$ , while the isotropic behavior is noted for small strains values up to 10%. It is important to mention that this same effect of strain on the trace of the WM can also be observed for  $n = 0$  and another excited Landau states, as shown in Figs. 4(a), (b), and (c). From Landau level  $n = 2$  we observe negative values in the WF that indicate non-classicality. This feature is usually observed for the WF of single photon states in quantum cavities [108]. The resemblance between effective Dirac-Weyl model in graphene and the Jaynes-Cummings model have been clearly established in Refs. [28–34]. This important connection between quantum optics systems and graphene can be useful as a key point in the

preparation of electron coherent states. For that reason, in the next subsection we study the phase-space representation of electron coherent states as well as its time evolution from the Heisenberg picture.

#### 4.1.3 Wigner and Husimi functions for electron coherent states $\Psi_\alpha(x, y)$

In order to observe the effect of strain on the WM for electron coherent states, we substitute the components of coherent states (33a) and (33b) into the integral matrix representation (34), getting:

$$W_\alpha(\vec{r}, \vec{p}) = \frac{\delta(p_y - k\hbar)}{(2 \exp(|\tilde{\alpha}|^2) - 1)} \begin{pmatrix} W_{11}(x, p_x) & -i\lambda W_{12}(x, p_x) \\ i\lambda W_{21}(x, p_x) & W_{22}(x, p_x) \end{pmatrix}, \quad (47)$$

where, by using properly Eq. (44), the matrix components are given by

$$W_{11}(\chi) = -\frac{e^{-\frac{1}{2}|\chi|^2}}{\pi} \sum_{n=1}^{\infty} \left[ \frac{(-|\tilde{\alpha}|^2)^n}{n!} L_{n-1}(|\chi|^2) + 2 \sum_{m=n+1}^{\infty} \frac{(-1)^n}{m!} \Re\{\tilde{\alpha}^n \tilde{\alpha}^{*m} \chi^{m-n}\} \sqrt{\frac{m}{n}} L_{n-1}^{m-n}(|\chi|^2) \right], \quad (48a)$$

$$W_{12}(\chi) = W_{21}^*(\chi) = \frac{1}{\pi} \exp\left(-\frac{1}{2}|\chi|^2 + \tilde{\alpha}^* \chi\right) \sum_{n=1}^{\infty} \frac{\tilde{\alpha}^n}{n!} \sqrt{n} (\chi^* - \tilde{\alpha}^*)^{n-1}, \quad (48b)$$

$$W_{22}(\chi) = \frac{1}{\pi} \exp\left(\frac{1}{2}|\chi|^2 - |\chi - \tilde{\alpha}|^2\right), \quad (48c)$$

where  $\Re(z)$  and  $\Im(z)$  denote the real and imaginary part of a complex number  $z$ , respectively. Expression (48c) corresponds to the scalar WF of a unnormalized coherent states as expected. The off-diagonal components can be interpreted like an interference term due to the superposition of the wave function of the electron from the sublattices A and B. Fig. 6 shows the trace of  $W_\alpha(\vec{r}, \vec{p})$  when the strain is applied in  $\mathcal{Z}$  and  $\mathcal{A}$  direction, respectively. It is observed that the trace of the WM also behaves as the stress-strain relationship of graphene. Since the compression of LLs favors the obtention of electron coherent states, we only consider positive strain values for the WM. Thus, the shape of the  $W_\alpha(\vec{r}, \vec{p})$ , by comparing deformations along the  $\mathcal{Z}$  and  $\mathcal{A}$  direction, is different in the nonlinear elastic regime. We can observe for  $\epsilon < 10\%$ , the WF has an identical response under the application of uniaxial strain in  $\mathcal{Z}$  and  $\mathcal{A}$  directions but with a difference of  $90^\circ$ . It is expected that the uncertainty relation is affected by the strain such as the distortion of classical energy orbits, (see Fig. 3). It is known that the coherent states keep their minimum values of uncertainty in position and linear momentum [10]. Herein, the positive strains along the  $\mathcal{Z}$  ( $\mathcal{A}$ ) direction increase (decrease) the uncertainty of  $p_x$  causing simultaneously decreasing (increasing) in the uncertainty of  $x$ , according to the amount  $\tau$  in Eq. (46). Therefore, the action of strain on electron coherent states in graphene is similar to the effect found in the squeezing of light coherent states in quantum optics [10].

On the other hand, when we change the parameter  $\alpha$  is possible to observe two main effects on the WF. First one, the increasing of  $|\alpha|^2$  shifts the maximum of the WF far away from the phase-space origin. This is identical to the displacement observed in light coherent states, where  $|\alpha|^2$  also corresponds to the average photon number [10]. Therefore, the quantity  $|\alpha|^2$  is

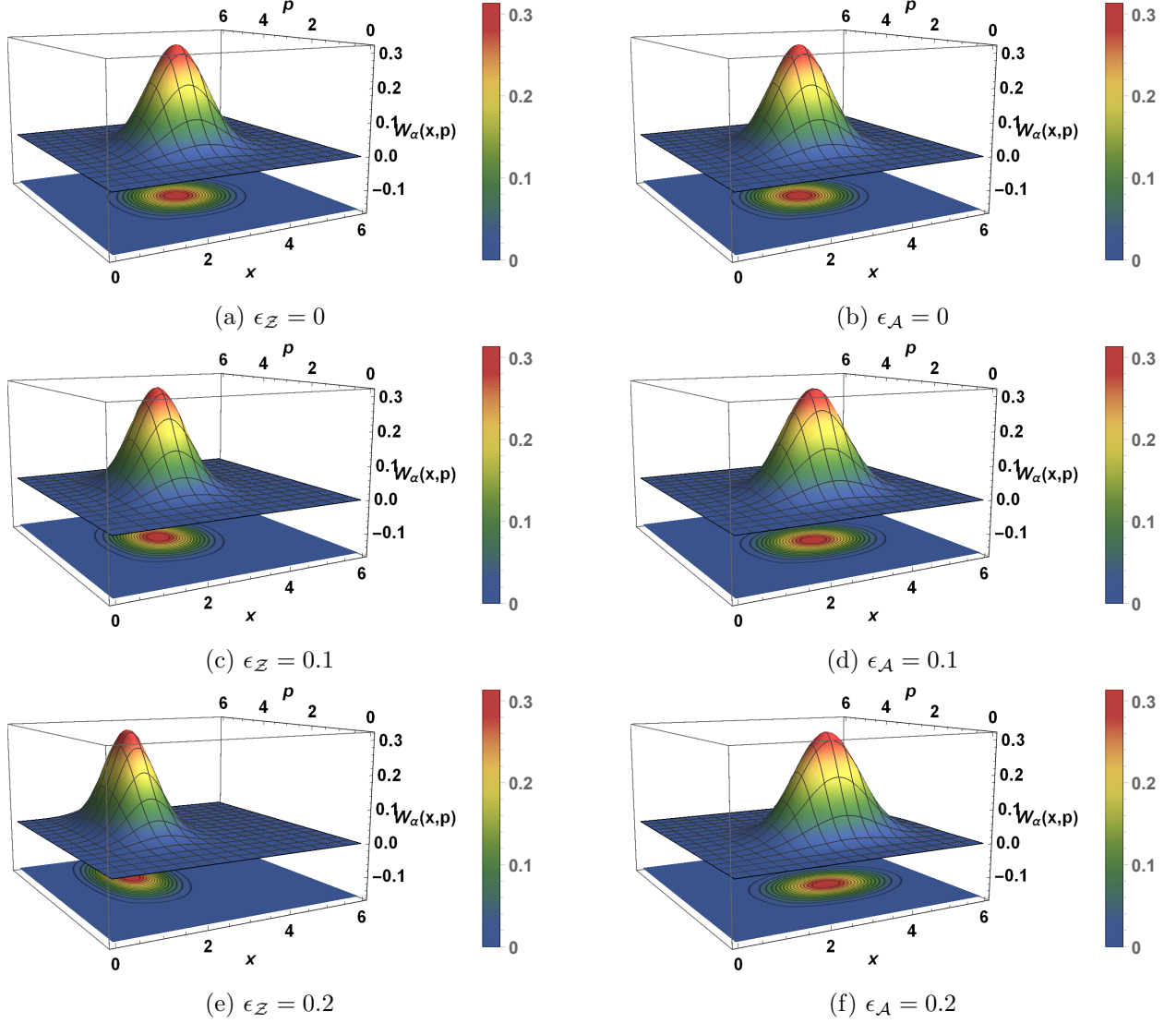


Figure 6: Trace of the Wigner matrix  $W_\alpha(\vec{r}, \vec{p})$  from Eq. (47) for deformations in zigzag ((a), (c), and (e)) and armchair directions ((b), (d), and (f)) using the set of values  $\alpha = 3 \exp(i\pi/4)$ ,  $B = 1$ ,  $k = \delta = 0$ , and different values of  $\epsilon$ .

proportional to the distance of the maximum of the WF for electron coherent state. Second one, it is also observed that the phase of  $\alpha$  causes rotations of the WF around the phase-space origin. However, we will show that the time evolution of electron states is very different to those ones of quantum optics.

#### 4.1.4 Time evolution of the Wigner matrix for electron coherent states

Now, we investigate the time evolution of the coherent states in phase space by applying the time evolution unitary operator  $U(t) = \exp(-iHt/\hbar)$  on the states  $\Psi_\alpha(x, y)$  in Eq. (32):

$$\Psi_\alpha(x, y, t) = U(t)\Psi_\alpha(x, y) = \frac{1}{\sqrt{2 \exp(|\tilde{\alpha}|^2) - 1}} \left[ \Psi_0(x, y) + \sum_{n=1}^{\infty} \frac{\sqrt{2} \tilde{\alpha}^n}{\sqrt{n!}} \exp(-iE_n t) \Psi_n(x, y) \right], \quad (49)$$

where  $E_n$  are the LLs (19). Hence, the expressions in (48) are recalculated and written respectively as

$$W_{11}(\chi, t) = -\frac{e^{-\frac{1}{2}|\chi|^2}}{\pi} \sum_{n=1}^{\infty} \left[ \frac{(-|\tilde{\alpha}|^2)^n}{n!} L_{n-1}(|\chi|^2) + 2 \sum_{m=n+1}^{\infty} \frac{(-1)^n}{m!} \chi^{m-n} A_{nm}(t) \sqrt{\frac{m}{n}} L_{n-1}^{m-n}(|\chi|^2) \right], \quad (50a)$$

$$W_{12}(\chi, t) = W_{21}^*(\chi, t) = \frac{e^{-\frac{1}{2}|\chi|^2}}{\pi} \sum_{n=0}^{\infty} \left[ \frac{\tilde{\alpha} |\tilde{\alpha}|^{2n}}{n! \sqrt{n+1}} (-1)^n e^{i(E_n - E_{n+1})t} L_n(|\chi|^2) + 2 \sum_{m=n+1}^{\infty} \frac{(-1)^n}{m! \sqrt{n+1}} \chi^{m-n} A_{n+1m}(t) L_{n-1}^{m-n}(|\chi|^2) \right], \quad (50b)$$

$$W_{22}(\chi, t) = \frac{e^{-\frac{1}{2}|\chi|^2}}{\pi} \left[ J_0(2i|\tilde{\alpha}\chi|) e^{-|\tilde{\alpha}|^2} + 2 \sum_{n=0}^{\infty} \sum_{m=n+1}^{\infty} \frac{(-1)^n}{m!} \chi^{m-n} A_{nm}(t) L_n^{m-n}(|\chi|^2) \right], \quad (50c)$$

where the temporal function  $A_{nm}(t) = \Re(\tilde{\alpha}^n \tilde{\alpha}^{*m} e^{i(E_m - E_n)t})$  has been defined and setting  $t = 0$  we recover the expressions (48). The  $A_{nm}(t)$  indicates that the trace of the WM changes its shape when the time increases due mainly to that  $E_n \propto \sqrt{n}$ . Since positive deformations tend to compress the LLs spectra, the time scale  $[0, T]$  ( $T$  denotes the rotation period) is also contracted as  $[0, \sqrt{ab}T]$ , while in light coherent states such a contraction does not exist because  $E_n \propto n$  and the eigenvalue  $\alpha$  evolves as  $\alpha(t) = \alpha \exp(i\omega t)$ . Also, it is known that for light coherent states the variation of the phase of  $\tilde{\alpha}$  causes only rotation of the corresponding WF around the phase-space origin without changing its shape [10]. However, the LLs dependency  $\sqrt{n}$  does not only produce rotation of the WM when the time is increased but also it generates oscillations, as shown in Fig. 7. We can observe that the maximum value of the WF remains in the time evolution changing its numerical value and turns around the origin, while negative values are observed through oscillations. This fact represents an important difference between the WFs of electron coherent states in graphene and the light ones in quantum optics. In the former case we observe that electron coherent states exhibit a quantum behavior, while in the latter the WF is always positive in anywhere point of phase-space. Nevertheless, the maximum value of the WF for both electron and photons describes closed orbits in phase-space. Besides, the time evolution of the WM trace reminds in a sense that of a particle in a Morse potential [109].

#### 4.1.5 Husimi function of electron coherent states

The Husimi function for the addressed problem can be construct as the probability of finding any coherent state with eigenvalue  $\alpha$  in another one with eigenvalue  $\alpha_0$  (see Eq. (40)). Therefore,



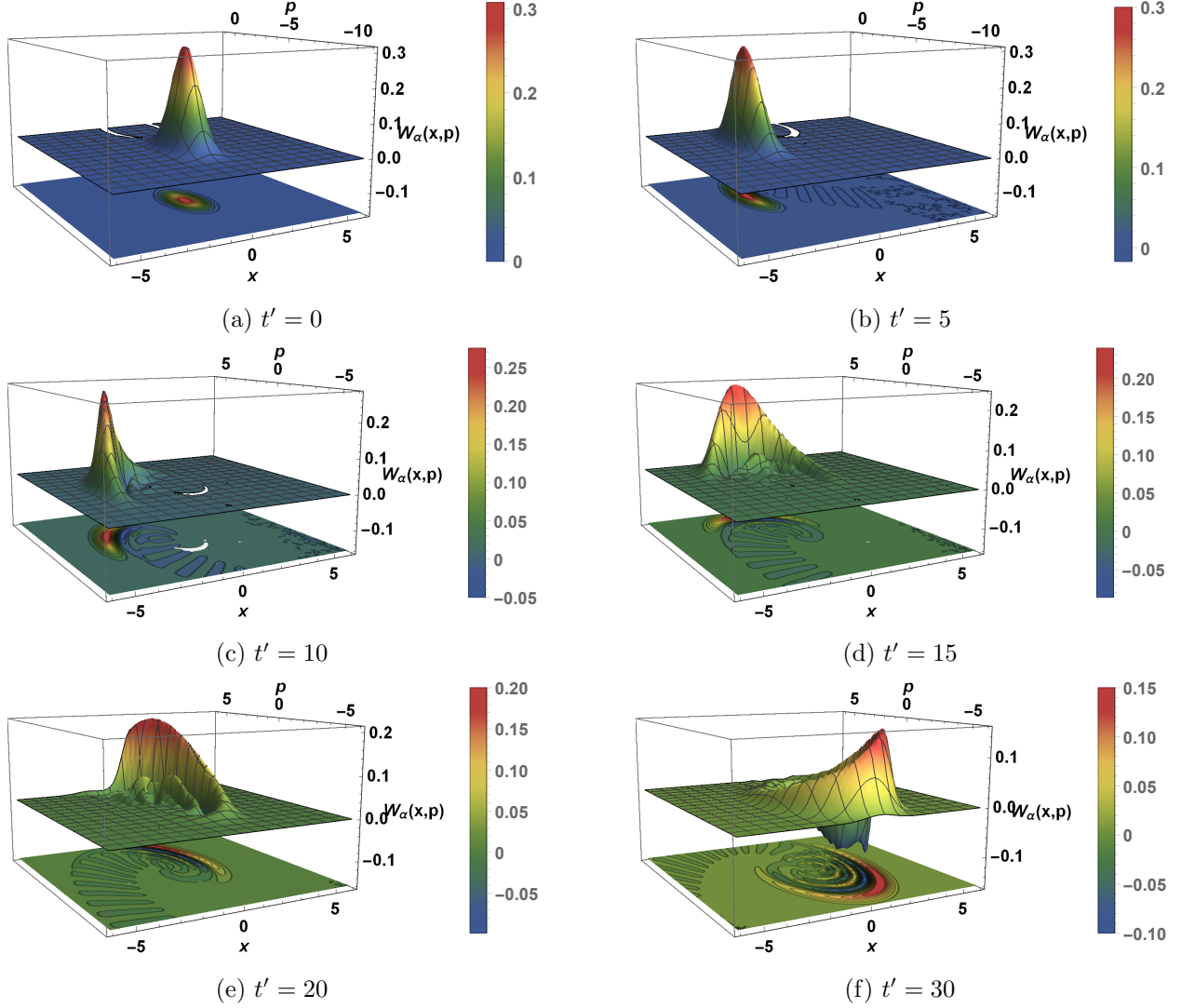


Figure 7: Time evolution of the trace of the WM  $W_\alpha(\vec{r}, \vec{p}, t)$  with  $\alpha = 3 \exp(-i\pi/2)$  and  $\epsilon = 0.2$  in  $\mathcal{Z}$  direction by using the components in Eq. (50). In all these cases  $B = 1$ ,  $k = \delta = 0$  and  $t' \equiv t/(v_F \sqrt{2e\hbar B})$ .

we have that (see Fig. (8)):

$$Q(\alpha) \equiv Q(\alpha, \alpha_0) = \frac{1}{\pi} |\langle \Psi_\alpha | \Psi_{\alpha_0} \rangle|^2 = \frac{1}{\pi} \frac{|2 \exp(\tilde{\alpha}^* \tilde{\alpha}_0) - 1|^2}{(2 \exp(|\tilde{\alpha}|^2) - 1)(2 \exp(|\tilde{\alpha}_0|^2) - 1)} > 0. \quad (51)$$

In contrast with the SHO, for which  $\langle x \rangle \propto \Re(\alpha)$  and  $\langle p_x \rangle \propto \Im(\alpha)$ , in the DW problem we cannot make a similar identification because the mean values of the position  $x$  and momentum  $p_x$  operators are related with the eigenvalue  $\alpha$  in a non-trivial form (see Ref. [93]). However, the  $Q(\alpha)$ -function (51) shows a smooth Gaussian-like shape as occurs for the SHO in phase-space, although its projection on the horizontal plane is a disk that does not preserve its shape for all



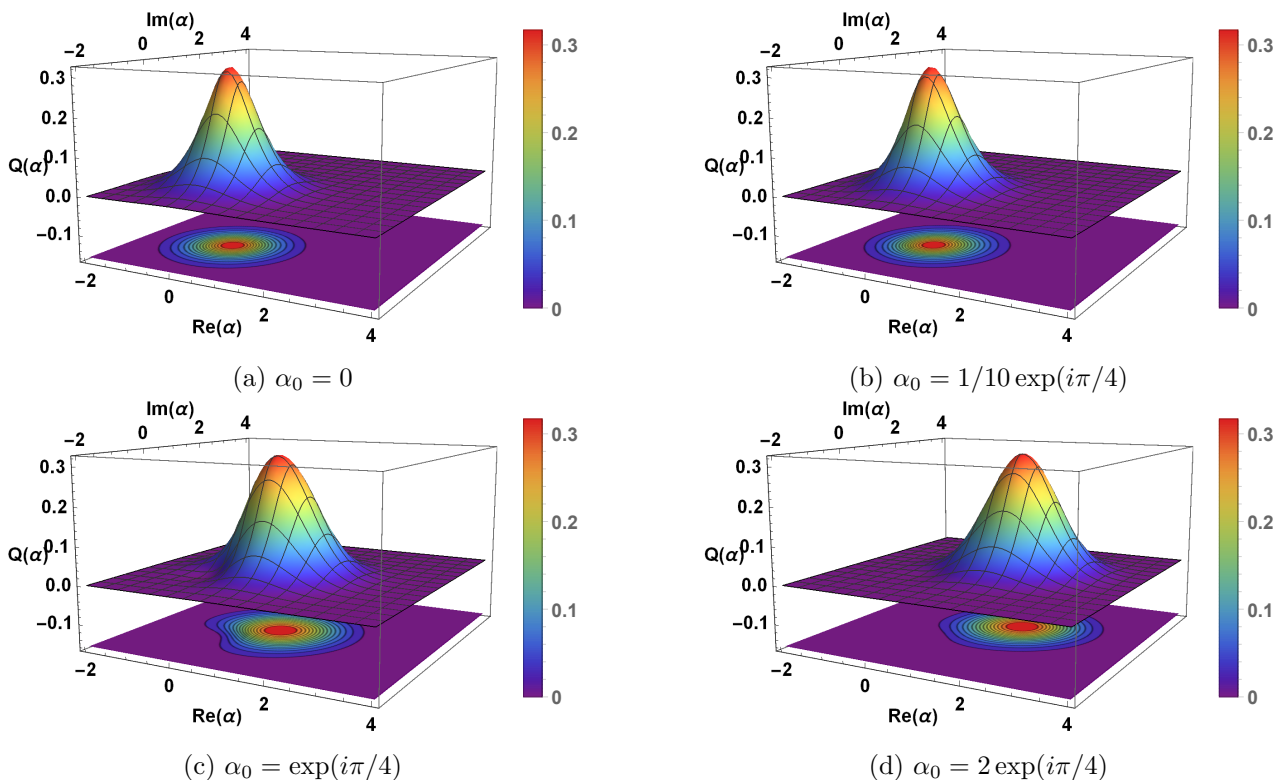


Figure 8: Husimi function  $Q(\alpha)$  for some values of  $\alpha_0$ . In all these cases  $B = 1$  and  $k = \delta = 0$ .

values of  $\alpha$ , as shown in Figs. 8(c) and (d). We think this fact is due to the spinorial nature of the solutions because each sublattice (A or B) has contributions to the Husimi function: for small values of  $|\alpha|$  only the wave function associated to an electron in sublattice B plays a part in the construction of  $Q(\alpha)$ , while as  $|\alpha|$  increases, a contribution of wave functions from both sublattices appears.

## 5 Conclusions and final remarks

We study the electron dynamics in uniaxially strained graphene in presence of a uniform and perpendicular magnetic field to the layer from a phase-space representation perspective. The Wigner matrix is a powerful theoretical tool that has been very useful for investigating quantum optics systems, quantum information, and been so far scarcely used for condensed matter. Since mechanical deformation modifies the atomic positions in the lattice and distorts the reciprocal space, Wigner matrix representation allows to evidence the effect of strain on the electron dynamics simultaneously in both spaces. Moreover, it indicates which electronic states present a non-classical behavior. This is of relevant importance for the realization of entanglement. By using tight-binding approach to nearest neighbors, it was possible to derive an effective Dirac-Weyl model, where we obtained Landau levels spectra and their corresponding wave functions. This effective model has a direct connection with other methods frequently used for studying

strained materials such as the geometrical approach [49], where an analytical expression of the geometrical parameters  $a$  and  $b$  as a function of the strain tensor components is found, as well as connection with the supersymmetric potential model [86]. Employing a generalized annihilation operator, we can build the electron coherent states from Landau ones and demonstrate that stretching along the zigzag direction favors the obtention of electron coherent states. We have found that the trace of the Wigner matrix for Landau and coherent states has different response when we apply uniaxial strain along the zigzag and armchair directions. Also, the time evolution of Wigner function evidences distinctive features between electronic and light quantum systems. We observe that the maximum value of this function describes closed orbits but, as time increases, the Wigner function shows negative values. This fact contrast with light coherent states, where positive values of the Wigner function are observed in the whole phase-space.

We think that our findings might help to establish protocols for the preparation of electron coherent states in the laboratory. Moreover, these results suggest the possibility of a feedback between electron and light quantum optics due to the analogy of approaches in condensed matter and quantum optics. Besides, it is worth to remark that the phase-space representation presented in this work has an advantage over canonical quantization, since it has allowed us to investigate the time evolution of electronic coherent states, which is difficult to perform using the notion of wave function because the energy spectrum (19) is not equidistant.

## Acknowledgments

YBO gratefully acknowledges financial support from CONACYT Proyecto Fronteras 952 and the UNAM-PAPIIT research grants IN-103017 and IA-101618. EDB acknowledges support from UPIIH of the National Polytechnic Institute (IPN, México). The authors also thank Thomas H. Seligman, Thomas Stegmann, Francois Leyvraz, Carlos A. González-Gutiérrez, Francisco J. Turrubiates, and Maurice Oliva-Leyva for helpful discussions, comments, and criticisms.

## A Wigner function: Moyal $\star$ -product

In this appendix, we present an alternative procedure to obtain the WF for the DW problem.

As was shown in above sections, the WF  $W(\vec{r}, \vec{p})$  is a real function defined in phase-space and deformation quantization formulation (DQF) provides an alternative method to obtain it. The implementation of the DQF on the study 1D quantum systems has allowed, in principle, to recover some previous results obtained from canonical quantization but described in phase-space.

In the QDF, the eigenvalue equation  $H\psi = E\psi$  is replaced by a  $\star$ -genvalue equation, namely:

$$H \star W = W \star H = EW, \quad (\text{A.1})$$

in order to describe the energy of an eigenstate with eigenvalue  $E$ , where the star-product ( $\star$ ) represents a deformation performed on the algebraic structure in phase-space of classical mechanics, which carries a non-commutative algebra in that of quantum mechanics.

One of the  $\star$ -products defined in the DQF framework is the so-called Moyal star-product ( $\star_M$ ) [110, 111]:

$$f \star_M g \equiv f \exp \left( \frac{i\hbar}{2} \left( \overleftarrow{\partial}_{\vec{r}} \overrightarrow{\partial}_{\vec{p}} + \overleftarrow{\partial}_{\vec{p}} \overrightarrow{\partial}_{\vec{r}} \right) \right) g, \quad (\text{A.2})$$

where  $\overleftarrow{\partial}$  ( $\overrightarrow{\partial}$ ) indicates that the derivative acts on the function to the left (right). Alternatively, the  $\star_M$ -product can be rewritten as

$$f(\vec{r}, \vec{p}) \star_M g(\vec{r}, \vec{p}) = f \left( \vec{r} + \frac{i\hbar}{2} \overrightarrow{\partial}_{\vec{p}}, \vec{p} - \frac{i\hbar}{2} \overrightarrow{\partial}_{\vec{r}} \right) g(\vec{r}, \vec{p}), \quad (\text{A.3a})$$

$$f(\vec{r}, \vec{p}) \star_M g(\vec{r}, \vec{p}) = f(\vec{r}, \vec{p}) g \left( \vec{r} - \frac{i\hbar}{2} \overleftarrow{\partial}_{\vec{p}}, \vec{p} + \frac{i\hbar}{2} \overleftarrow{\partial}_{\vec{r}} \right). \quad (\text{A.3b})$$

Thus, the WF satisfies the  $\star_M$ -genvalue equations

$$H(\vec{r}, \vec{p}) \star_M W(\vec{r}, \vec{p}) = H \left( \vec{r} + \frac{i\hbar}{2} \overrightarrow{\partial}_{\vec{p}}, \vec{p} - \frac{i\hbar}{2} \overrightarrow{\partial}_{\vec{r}} \right) W(\vec{r}, \vec{p}) = EW(\vec{r}, \vec{p}), \quad (\text{A.4a})$$

$$H(\vec{r}, \vec{p}) \star_M W(\vec{r}, \vec{p}) = W(\vec{r}, \vec{p}) H \left( \vec{r} - \frac{i\hbar}{2} \overleftarrow{\partial}_{\vec{p}}, \vec{p} + \frac{i\hbar}{2} \overleftarrow{\partial}_{\vec{r}} \right) = EW(\vec{r}, \vec{p}), \quad (\text{A.4b})$$

where  $E$  is the energy eigenvalue of  $H\psi = E\psi$ .

According to [107], we can solve the Dirac-Weyl equation (12) by applying the Moyal  $\star$ -product:

$$H_D(\vec{r}, \vec{p}) \star W(\vec{r}, \vec{p}) = EW(\vec{r}, \vec{p}), \quad (\text{A.5})$$

where

$$W(\vec{r}, \vec{p}) = \begin{pmatrix} W^{(a)}(\vec{r}, \vec{p}) & 0 \\ 0 & W^{(b)}(\vec{r}, \vec{p}) \end{pmatrix}, \quad W^{(a,b)}(\vec{r}, \vec{p}) = \begin{pmatrix} W_{11}^{(a,b)}(\vec{r}, \vec{p}) & W_{12}^{(a,b)}(\vec{r}, \vec{p}) \\ W_{21}^{(a,b)}(\vec{r}, \vec{p}) & W_{22}^{(a,b)}(\vec{r}, \vec{p}) \end{pmatrix}. \quad (\text{A.6})$$

This means that the WF actually is a  $4 \times 4$  matrix but that in an adequate representation can be reduced to a diagonal partitioned matrix as is shown in Eq. (A.6) [107]. Here, the  $2 \times 2$  WM  $W^{(a)}(\vec{r}, \vec{p})$  would correspond to Dirac fermions at  $K_D$  valley, while  $W^{(b)}(\vec{r}, \vec{p})$  to those at  $K'_D$  valley, so that we will just focus in the former.

Equation (A.5) gives rise to two decoupled equations:

$$v_F (a\sigma_x [p_x + eA_x] + b\sigma_y [p_y + eA_y]) \star W^{(b)} = EW^{(a)}, \quad (\text{A.7a})$$

$$v_F (a\sigma_x [p_x + eA_x] + b\sigma_y [p_y + eA_y]) \star W^{(a)} = EW^{(b)}. \quad (\text{A.7b})$$

After decoupling the above expressions, we obtain the following  $\star$ -genvalue equation for  $W^{(a)}(\vec{r}, \vec{p})$ :

$$\begin{aligned} H_D^{(a)} \star W^{(a)} &= [v_F (a\sigma_x [p_x + eA_x] + b\sigma_y [p_y + eA_y])] \star \\ &\star [v_F (a\sigma_x [p_x + eA_x] + b\sigma_y [p_y + eA_y])] \star W^{(a)} = E^2 W^{(a)}, \end{aligned} \quad (\text{A.8})$$

where  $[W^{(a)}(\vec{r}, \vec{p})]_{ij} \equiv W_{ij}(x, p_x)W_{ij}(y, p_y)$ ,  $i, j = 1, 2$ .

Considering the Landau gauge  $\vec{A} = B_0 x \hat{e}_y$  and the Bopp's shift (Eq. (A.3a)), the Hamiltonian  $H_D^{(a)}$  can be rewritten as:

$$\begin{aligned} H_D^{(a)} &= v_F^2 \hbar^2 \left[ a \sigma_x \left( \frac{p_x}{\hbar} - \frac{i}{2} \partial_x \right) + b \sigma_y \left[ \left( \frac{p_y}{\hbar} - \frac{i}{2} \partial_y \right) + \frac{e B_0}{\hbar} \left( x + \frac{i \hbar}{2} \partial_{p_x} \right) \right] \right]^2 \\ &= a b v_F^2 \hbar^2 \left\{ \left[ \zeta \left( \frac{p_x^2}{\hbar^2} - \frac{1}{4} \partial_x^2 \right) + \zeta^{-1} \left( \frac{p_y}{\hbar} + \frac{\omega_B}{2} x \right)^2 - \frac{1}{4} \zeta^{-1} \left( \frac{\omega_B \hbar}{2} \partial_{p_x} - \partial_y \right)^2 \right] \mathbb{I} + \frac{\omega_B}{2} \sigma_z \right. \\ &\quad \left. + i \left[ -\zeta \frac{p_x}{\hbar} \partial_x + \zeta^{-1} \left( \frac{p_y}{\hbar} + \frac{\omega_B}{2} x \right) \left( \frac{\omega_B \hbar}{2} \partial_{p_x} - \partial_y \right) \right] \mathbb{I} \right\}, \end{aligned} \quad (\text{A.9})$$

where  $\mathbb{I}$  is the  $2 \times 2$  identity matrix,  $\omega_B = \zeta \omega_\zeta$  and  $\sigma_z$  is the third Pauli matrix. Here, we could assume that the corresponding pseudo-spinor is an eigenstate of the operator  $\sigma_z$  in order to reduce the WF to a diagonal matrix; however, we will work with the entire representation.

By defining the quantities

$$\mathcal{E}_1 = \frac{E^2}{a b v_F^2 \hbar^2} - \frac{\omega_B}{2}, \quad \mathcal{E}_2 = \frac{E^2}{a b v_F^2 \hbar^2} + \frac{\omega_B}{2}. \quad (\text{A.10})$$

and using the variables  $\xi$  and  $s$  defined in (43), we can obtain the following pair of Hamiltonians:

$$H_1 = \frac{\omega_B}{2} \left[ s^2 + \left( \sqrt{\frac{2}{\zeta \omega_B}} \left( \frac{p_y}{\hbar} - k \right) + \xi \right)^2 - \frac{1}{4} \partial_\xi^2 - \frac{1}{4} \left( \partial_s - \sqrt{\frac{2}{\zeta \omega_B}} \partial_y \right)^2 \right], \quad (\text{A.11a})$$

$$H_2 = \frac{\omega_B}{2} \left[ -s \partial_\xi + \left( \sqrt{\frac{2}{\zeta \omega_B}} \left( \frac{p_y}{\hbar} - k \right) + \xi \right) \left( \partial_s - \sqrt{\frac{2}{\zeta \omega_B}} \partial_y \right) \right]. \quad (\text{A.11b})$$

Following the *ansatz* shown in [9] for the WF  $W_{ij}(y, p_y)$ , the solutions for the problem in Eq. (A.8) are given as

$$W(p_y) \equiv W_{ij}(y, p_y) = \delta(p_y - k \hbar), \quad i, j = 1, 2, \quad (\text{A.12a})$$

$$W_{1j}(x, p_x) = \frac{(-1)^{n-1}}{\pi} \exp \left( -\frac{1}{2} |\chi|^2 \right) L_{n-1}(|\chi|^2), \quad j = 1, 2, \quad (\text{A.12b})$$

$$W_{2j}(x, p_x) = \frac{(-1)^n}{\pi} \exp \left( -\frac{1}{2} |\chi|^2 \right) L_n(|\chi|^2), \quad j = 1, 2, \quad (\text{A.12c})$$

where again  $\chi = \sqrt{2}(\xi + is)$ , and the corresponding energy spectrum turns out to be

$$E_{2,0} = 0, \quad E_{2,n} = E_{1,n-1} = \text{sgn}(n) v_F' \hbar \sqrt{\omega_B |n|}, \quad (\text{A.13})$$

$n = 0, \pm 1, \pm 2, \dots$ ,  $\text{sgn}(0) = 1$  and  $v_F' = \sqrt{ab} v_F$ . Meanwhile, the  $2 \times 2$  Wigner matrices in (A.6) can be rewritten as

$$W^{(a,b)}(\vec{r}, \vec{p}) = \frac{1}{2^{(1-\delta_{0n})}} \begin{pmatrix} W_{11}^{(a,b)}(\vec{r}, \vec{p}) & W_{12}^{(a,b)}(\vec{r}, \vec{p}) \\ W_{21}^{(a,b)}(\vec{r}, \vec{p}) & W_{22}^{(a,b)}(\vec{r}, \vec{p}) \end{pmatrix}, \quad (\text{A.14})$$

where the components are the following WFs:

$$W_{11}^{(a,b)}(\vec{r}, \vec{p}) = W_{12}^{(a,b)}(\vec{r}, \vec{p}) = (1 - \delta_{0n}) \frac{(-1)^{n-1}}{\pi} \delta(p_y - k\hbar) \exp\left(-\frac{1}{2}|\chi|^2\right) L_{n-1}(|\chi|^2), \quad (\text{A.15a})$$

$$W_{21}^{(a,b)}(\vec{r}, \vec{p}) = W_{22}^{(a,b)}(\vec{r}, \vec{p}) = \frac{(-1)^n}{\pi} \delta(p_y - k\hbar) \exp\left(-\frac{1}{2}|\chi|^2\right) L_n(|\chi|^2), \quad (\text{A.15b})$$

such that

$$\int_{-\infty}^{\infty} \int_{-\infty}^{\infty} \text{Tr} [W^{(a,b)}(\vec{r}, \vec{p})] d\vec{r} d\vec{p} = 1. \quad (\text{A.16})$$

Notice that the factor  $(1 - \delta_{0n})$  in Eqs. (A.14) and (A.15a) guaranties that such expressions satisfy the  $\star$ -genvalue equation (A.8) for the Landau level  $n = 0$ .

## A.1 Comparison with the integral representation

Coming back to WF obtained by the integral representation (Eq. (41)), we can identify each component in Eq. (45) with the given ones in (A.15), except the off-diagonal terms,

$$W_{12}^{(a,b)}(\vec{r}, \vec{p}) \neq W_{n-1,n}(\vec{r}, \vec{p}), \quad W_{21}^{*(a,b)}(\vec{r}, \vec{p}) \neq W_{n,n-1}(\vec{r}, \vec{p}). \quad (\text{A.17})$$

This is because in both representations the trace of the WF is an invariant, while the off-diagonal terms depend on which representation is considered.

However, we can establish a connection between two representations as follows. By acting the Hamiltonians in Eq. (A.11) on the above expressions and recalling that  $f(x)\delta(x-a) = f(a)\delta(x-a)$ , we get:

$$\left(H_1 + \frac{\omega_B}{2}\right) W_{n-1,n}(\vec{r}, \vec{p}) = \left(n + \frac{1}{2}\right) \omega_B W_{n-1,n}(\vec{r}, \vec{p}), \quad H_2 W_{n-1,n}(\vec{r}, \vec{p}) = i \frac{\omega_B}{2} W_{n-1,n}(\vec{r}, \vec{p}), \quad (\text{A.18a})$$

$$\left(H_1 - \frac{\omega_B}{2}\right) W_{n,n-1}(\vec{r}, \vec{p}) = \left(n - \frac{1}{2}\right) \omega_B W_{n,n-1}(\vec{r}, \vec{p}), \quad H_2 W_{n,n-1}(\vec{r}, \vec{p}) = -i \frac{\omega_B}{2} W_{n,n-1}(\vec{r}, \vec{p}). \quad (\text{A.18b})$$

By taking the complex conjugate of Eqs. (??) and (??) and adding it to (A.18a) and (A.18b), respectively, we have that

$$H_1 \Re[W_{n-1,n}(\vec{r}, \vec{p})] = n\omega_B \Re[W_{n-1,n}(\vec{r}, \vec{p})], \quad H_2 \Re[W_{n-1,n}(\vec{r}, \vec{p})] = 0. \quad (\text{A.19})$$

Therefore, although separately the off-diagonal terms of the WF  $W_n(\vec{r}, \vec{p})$  in Eq. (41) are not solutions of the  $\star$ -genvalue equation (A.8), their real part is. Thus, the integral representation of the WF also gives rise to a matrix function but in another representation.

## References

- [1] L. D. Landau and E. M. Lifshits, *Quantum mechanics: non-relativistic theory*. Butterworth-Heinemann, 1977.
- [2] E. Wigner, “On the quantum correction for thermodynamic equilibrium,” *Phys. Rev.*, vol. 40, pp. 749–759, Jun 1932.
- [3] M. Hillery, R. O’Connell, M. Scully, and E. Wigner, “Distribution functions in physics: Fundamentals,” *Phys. Rep.*, vol. 106, no. 3, pp. 121 – 167, 1984.
- [4] K. E. Cahill and R. J. Glauber, “Density Operators and Quasiprobability Distributions,” *Phys. Rev.*, vol. 177, pp. 1882–1902, Jan 1969.
- [5] A. Kenfack and K. Życzkowski, “Negativity of the Wigner function as an indicator of non-classicality,” *J. Opt. B: Quantum Semiclassical Opt.*, vol. 6, pp. 396–404, aug 2004.
- [6] K. Husimi, “Some formal properties of the density matrix,” *Proc. Phys. Math. Soc. Jpn.*, vol. 22, no. 4, pp. 264–314, 1940.
- [7] W. B. Case, “Wigner functions and Weyl transforms for pedestrians,” *Am. J. Phys.*, vol. 76, no. 10, pp. 937–946, 2008.
- [8] J. Weinbub and D. K. Ferry, “Recent advances in Wigner function approaches,” *Appl. Phys. Rev.*, vol. 5, no. 4, p. 041104, 2018.
- [9] S. Kryukov and M. Walton, “On infinite walls in deformation quantization,” *Ann. Phys.*, vol. 317, no. 2, pp. 474 – 491, 2005.
- [10] C. Gerry and P. L. Knight, *Introductory quantum optics*. Cambridge University Press, 2005.
- [11] R. H. H. L. S. Ding, G. Maslennikov and D. Matsukevich, “Quantum parametric oscillator with trapped ions,” *Phys. Rev. Lett.*, vol. 119, p. 150404, Oct 2017.
- [12] D. Leiner, R. Zeier, and S. J. Glaser, “Wigner tomography of multispin quantum states,” *Phys. Rev. A*, vol. 96, p. 063413, Dec 2017.
- [13] X. Gu, A. F. Kockum, A. Miranowicz, Y.-X. Liu, and F. Nori, “Microwave photonics with superconducting quantum circuits,” *Phys. Rep.*, vol. 718-719, pp. 1 – 102, 2017. Microwave photonics with superconducting quantum circuits.
- [14] E. Knyazev, K. Y. Spasibko, M. V. Chekhova, and F. Y. Khalili, “Quantum tomography enhanced through parametric amplification,” *New J. Phys.*, vol. 20, p. 013005, jan 2018.
- [15] D. Ferraro, B. Roussel, C. Cabart, E. Thibierge, G. Fève, C. Grenier, and P. Degiovanni, “Real-Time Decoherence of Landau and Levitov Quasiparticles in Quantum Hall Edge Channels,” *Phys. Rev. Lett.*, vol. 113, p. 166403, Oct 2014.

- [16] A. Marguerite, E. Bocquillon, J.-M. Berroir, B. Plaçais, A. Cavanna, Y. Jin, P. Degiovanni, and G. Fève, “Two-particle interferometry in quantum Hall edge channels,” *Phys. Status Solidi B*, vol. 254, no. 3, p. 1600618, 2017.
- [17] R. Birrittella, K. Cheng, and C. C. Gerry, “Photon-number parity oscillations in the resonant Jaynes-Cummings model,” *Opt. Commun.*, vol. 354, pp. 286 – 290, 2015.
- [18] R. P. Rundle, P. W. Mills, T. Tilma, J. H. Samson, and M. J. Everitt, “Simple procedure for phase-space measurement and entanglement validation,” *Phys. Rev. A*, vol. 96, p. 022117, Aug 2017.
- [19] C. A. González-Gutiérrez and J. M. Torres, “Atomic Bell measurement via two-photon interactions,” *Phys. Rev. A*, vol. 99, p. 023854, Feb 2019.
- [20] C. Jacoboni and P. Bordone, “The Wigner function approach to non-equilibrium electron transport,” *Rep. Prog. Phys.*, vol. 67, pp. 1033–1071, jun 2004.
- [21] C. Buerle, D. C. Glatli, T. Meunier, F. Portier, P. Roche, P. Roulleau, S. Takada, and X. Waintal, “Coherent control of single electrons: a review of current progress,” *Rep. Prog. Phys.*, vol. 81, p. 056503, apr 2018.
- [22] D. Ferraro, T. Jonckheere, J. Rech, and T. Martin, “Electronic quantum optics beyond the integer quantum Hall effect,” *Phys. Status Solidi B*, vol. 254, no. 3, p. 1600531, 2017.
- [23] O. Morandi and F. Schrrer, “Wigner model for quantum transport in graphene,” *J. Phys. A: Math. Theor.*, vol. 44, p. 265301, may 2011.
- [24] T. Jullien, P. Roulleau, B. Roche, A. Cavanna, Y. Jin, and D. C. Glatli, “Quantum tomography of an electron,” *Nature*, vol. 514, p. 603, oct 2014.
- [25] D. J. Mason, M. F. Borunda, and E. J. Heller, “Semiclassical deconstruction of quantum states in graphene,” *Phys. Rev. B*, vol. 88, p. 165421, Oct 2013.
- [26] G. J. Iafrate, V. N. Sokolov, and J. B. Krieger, “Quantum transport and the Wigner distribution function for Bloch electrons in spatially homogeneous electric and magnetic fields,” *Phys. Rev. B*, vol. 96, p. 144303, Oct 2017.
- [27] D. K. Ferry and I. Welland, “Relativistic Wigner functions in transition metal dichalcogenides,” *J. Comput. Electron.*, vol. 17, pp. 110–117, Mar 2018.
- [28] D. Ojeda-Guillén, R. D. Mota, and V. D. Granados, “A generalized Jaynes-Cummings model: The relativistic parametric amplifier and a single trapped ion,” *J. Math. Phys.*, vol. 57, no. 6, p. 062104, 2016.
- [29] E. Chorenó and D. Ojeda-Guillén and M. Salazar-Ramírez and V.D. Granados, “Two-mode generalization of the Jaynes-Cummings and Anti-Jaynes-Cummings models,” *Ann. Phys.*, vol. 387, pp. 121 – 134, 2017.



- [30] A. Jellal, A. E. Mouhafid, and M. Daoud, “Massless Dirac fermions in an electromagnetic field,” *J. Stat. Mech.: Theory Exp.*, vol. 2012, p. P01021, jan 2012.
- [31] T. M. Rusin and W. Zawadzki, “Zitterbewegung of electrons in graphene in a magnetic field,” *Phys. Rev. B*, vol. 78, p. 125419, Sep 2008.
- [32] B. Dóra, K. Ziegler, P. Thalmeier, and M. Nakamura, “Rabi Oscillations in Landau-Quantized Graphene,” *Phys. Rev. Lett.*, vol. 102, p. 036803, Jan 2009.
- [33] N. Goldman, A. Kubasiak, A. Bermudez, P. Gaspard, M. Lewenstein, and M. A. Martin-Delgado, “Non-Abelian Optical Lattices: Anomalous Quantum Hall Effect and Dirac Fermions,” *Phys. Rev. Lett.*, vol. 103, p. 035301, Jul 2009.
- [34] J. Schliemann, “Cyclotron motion in graphene,” *New J. Phys.*, vol. 10, p. 043024, apr 2008.
- [35] V. M. Pereira, A. H. Castro Neto, and N. M. R. Peres, “Tight-binding approach to uniaxial strain in graphene,” *Phys. Rev. B*, vol. 80, p. 045401, Jul 2009.
- [36] V. M. Pereira and A. H. Castro Neto, “Strain Engineering of Graphene’s Electronic Structure,” *Phys. Rev. Lett.*, vol. 103, p. 046801, Jul 2009.
- [37] V. M. Pereira, R. M. Ribeiro, N. M. R. Peres, and A. H. C. Neto, “Optical properties of strained graphene,” *Europhys. Lett. EPL*, vol. 92, p. 67001, dec 2010.
- [38] G. Cocco, E. Cadelano, and L. Colombo, “Gap opening in graphene by shear strain,” *Phys. Rev. B*, vol. 81, p. 241412, Jun 2010.
- [39] R. M. Ribeiro, V. M. Pereira, N. M. R. Peres, P. R. Briddon, and A. H. C. Neto, “Strained graphene: tight-binding and density functional calculations,” *New J. Phys.*, vol. 11, p. 115002, nov 2009.
- [40] E. Cadelano, P. L. Palla, S. Giordano, and L. Colombo, “Nonlinear Elasticity of Monolayer Graphene,” *Phys. Rev. Lett.*, vol. 102, p. 235502, Jun 2009.
- [41] L. Colombo and S. Giordano, “Nonlinear elasticity in nanostructured materials,” *Rep. Prog. Phys.*, vol. 74, p. 116501, oct 2011.
- [42] A. H. Castro Neto, F. Guinea, N. M. R. Peres, K. S. Novoselov, and A. K. Geim, “The electronic properties of graphene,” *Rev. Mod. Phys.*, vol. 81, pp. 109–162, Jan 2009.
- [43] T. Stegmann and N. Szpak, “Current flow paths in deformed graphene: from quantum transport to classical trajectories in curved space,” *New J. Phys.*, vol. 18, p. 053016, may 2016.
- [44] T. Stegmann and N. Szpak, “Current splitting and valley polarization in elastically deformed graphene,” *2D Materials*, vol. 6, p. 015024, dec 2018.

- [45] F. Zhai, Y. Ma, and K. Chang, “Valley beam splitter based on strained graphene,” *New J. Phys.*, vol. 13, p. 083029, aug 2011.
- [46] Z. Wu, F. Zhai, F. M. Peeters, H. Q. Xu, and K. Chang, “Valley-Dependent Brewster Angles and Goos-Hänchen Effect in Strained Graphene,” *Phys. Rev. Lett.*, vol. 106, p. 176802, Apr 2011.
- [47] V. H. Nguyen, S. Dechamps, P. Dollfus, and J.-C. Charlier, “Valley Filtering and Electronic Optics Using Polycrystalline Graphene,” *Phys. Rev. Lett.*, vol. 117, p. 247702, Dec 2016.
- [48] M. Settnes, S. R. Power, M. Brandbyge, and A.-P. Jauho, “Graphene nanobubbles as valley filters and beam splitters,” *Phys. Rev. Lett.*, vol. 117, p. 276801, Dec 2016.
- [49] Y. Betancur-Ocampo, M. Cifuentes-Quintal, G. Cordourier-Maruri, and R. de Coss, “Landau levels in uniaxially strained graphene: A geometrical approach,” *Ann. Phys.*, vol. 359, pp. 243 – 251, 2015.
- [50] Y. Betancur-Ocampo, “Partial positive refraction in asymmetric Veselago lenses of uniaxially strained graphene,” *Phys. Rev. B*, vol. 98, p. 205421, Nov 2018.
- [51] Y. Betancur-Ocampo, “Controlling electron flow in anisotropic Dirac materials heterojunctions: a super-diverging lens,” *J. Phys.: Condens. Matter*, vol. 30, p. 435302, oct 2018.
- [52] B. Amorim, A. Cortijo, F. de Juan, A. Grushin, F. Guinea, A. Gutierrez-Rubio, H. Ochoa, V. Parente, R. Roldán, P. San-Jose, J. Schiefele, M. Sturla, and M. Vozmediano, “Novel effects of strains in graphene and other two dimensional materials,” *Phys. Rep.*, vol. 617, pp. 1 – 54, 2016.
- [53] M. Oliva-Leyva and G. G. Naumis, “Understanding electron behavior in strained graphene as a reciprocal space distortion,” *Phys. Rev. B*, vol. 88, p. 085430, Aug 2013.
- [54] G. G. Naumis, S. Barraza-Lopez, M. Oliva-Leyva, and H. Terrones, “Electronic and optical properties of strained graphene and other strained 2D materials: a review,” *Rep. Prog. Phys.*, vol. 80, p. 096501, aug 2017.
- [55] M. Oliva-Leyva and G. G. Naumis, “Tunable dichroism and optical absorption of graphene by strain engineering,” *2D Mater.*, vol. 2, p. 025001, apr 2015.
- [56] R. Carrillo-Bastos, C. León, D. Faria, A. Latgé, E. Y. Andrei, and N. Sandler, “Strained fold-assisted transport in graphene systems,” *Phys. Rev. B*, vol. 94, p. 125422, Sep 2016.
- [57] E. Andrade, R. Carrillo-Bastos, and G. G. Naumis, “Valley engineering by strain in Kekulé-distorted graphene,” *Phys. Rev. B*, vol. 99, p. 035411, Jan 2019.

- [58] S. Barraza-Lopez and A. A. Pacheco Sanjuan and Z. Wang and M. Vanević, “Strain-engineering of graphene’s electronic structure beyond continuum elasticity,” *Solid State Commun.*, vol. 166, pp. 70 – 75, 2013.
- [59] F. M. D. Pellegrino, G. G. N. Angilella, and R. Pucci, “Strain effect on the optical conductivity of graphene,” *Phys. Rev. B*, vol. 81, p. 035411, Jan 2010.
- [60] M. Vozmediano, M. Katsnelson, and F. Guinea, “Gauge fields in graphene,” *Phys. Rep.*, vol. 496, no. 4, pp. 109 – 148, 2010.
- [61] F. Guinea, M. I. Katsnelson, and A. K. Geim, “Energy gaps and a zero-field quantum Hall effect in graphene by strain engineering,” *Nat. Phys.*, vol. 6, no. 1, pp. 30–33, 2010.
- [62] E. Arias, A. R. Hernández, and C. Lewenkopf, “Gauge fields in graphene with nonuniform elastic deformations: A quantum field theory approach,” *Phys. Rev. B*, vol. 92, p. 245110, Dec 2015.
- [63] J. V. Sloan, A. A. P. Sanjuan, Z. Wang, C. Horvath, and S. Barraza-Lopez, “Strain gauge fields for rippled graphene membranes under central mechanical load: An approach beyond first-order continuum elasticity,” *Phys. Rev. B*, vol. 87, p. 155436, Apr 2013.
- [64] M. Settnes, S. R. Power, and A.-P. Jauho, “Pseudomagnetic fields and triaxial strain in graphene,” *Phys. Rev. B*, vol. 93, p. 035456, Jan 2016.
- [65] K. K. Gomes, W. Mar, W. Ko, F. Guinea, and H. C. Manoharan, “Designer Dirac fermions and topological phases in molecular graphene,” *Nature*, vol. 483, p. 306, mar 2012.
- [66] N. Levy, S. A. Burke, K. L. Meaker, M. Panlasigui, A. Zettl, F. Guinea, A. H. C. Neto, and M. F. Crommie, “Strain-Induced Pseudo-Magnetic Fields Greater Than 300 Tesla in Graphene Nanobubbles,” *Science*, vol. 329, no. 5991, pp. 544–547, 2010.
- [67] M. C. Rechtsman, J. M. Zeuner, A. Tünnermann, S. Nolte, M. Segev, and A. Szameit, “Strain-induced pseudomagnetic field and photonic Landau levels in dielectric structures,” *Nat. Photonics*, vol. 7, p. 153, dec 2012.
- [68] Y. S. Ang, S. A. Yang, C. Zhang, Z. Ma, and L. K. Ang, “Valleytronics in merging Dirac cones: All-electric-controlled valley filter, valve, and universal reversible logic gate,” *Phys. Rev. B*, vol. 96, p. 245410, Dec 2017.
- [69] S.-M. Choi, S.-H. Jhi, and Y.-W. Son, “Effects of strain on electronic properties of graphene,” *Phys. Rev. B*, vol. 81, p. 081407, Feb 2010.
- [70] I. I. Naumov and A. M. Bratkovsky, “Gap opening in graphene by simple periodic inhomogeneous strain,” *Phys. Rev. B*, vol. 84, p. 245444, Dec 2011.
- [71] H. Rostami and R. Asgari, “Electronic ground-state properties of strained graphene,” *Phys. Rev. B*, vol. 86, p. 155435, Oct 2012.

- [72] M. Deng, Y.-J. Wang, Y. Gang, and J.-F. Chen, “Effect of uniaxial strain on the electronic transport through disordered graphene pn junctions,” *Mod. Phys. Lett. B*, vol. 30, no. 26, p. 1650337, 2016.
- [73] H. Shioya, M. F. Craciun, S. Russo, M. Yamamoto, and S. Tarucha, “Straining graphene using thin film shrinkage methods,” *Nano Lett.*, vol. 14, no. 3, pp. 1158–1163, 2014. PMID: 24490629.
- [74] H. Shioya, S. Russo, M. Yamamoto, M. F. Craciun, and S. Tarucha, “Electron states of uniaxially strained graphene,” *Nano Lett.*, vol. 15, no. 12, pp. 7943–7948, 2015. PMID: 26619326.
- [75] R. Beams, L. G. Cançado, A. Jorio, A. N. Vamivakas, and L. Novotny, “Tip-enhanced Raman mapping of local strain in graphene,” *Nanotechnology*, vol. 26, p. 175702, apr 2015.
- [76] S.-M. Lee, S.-M. Kim, M. Y. Na, H. J. Chang, K.-S. Kim, H. Yu, H.-J. Lee, and J.-H. Kim, “Materialization of strained CVD-graphene using thermal mismatch,” *Nano Res.*, vol. 8, pp. 2082–2091, Jun 2015.
- [77] F. Colangelo, A. Pitanti, V. Mišeikis, C. Coletti, P. Pingue, D. Pisignano, F. Beltram, A. Tredicucci, and S. Roddaro, “Controlling local deformation in graphene using micro-metric polymeric actuators,” *2D Mater.*, vol. 5, p. 045032, sep 2018.
- [78] M. Assili, S. Haddad, and W. Kang, “Electric field-induced valley degeneracy lifting in uniaxial strained graphene: Evidence from magnetophonon resonance,” *Phys. Rev. B*, vol. 91, p. 115422, Mar 2015.
- [79] D. Midtvedt, C. H. Lewenkopf, and A. Croy, “Strain–displacement relations for strain engineering in single-layer 2D materials,” *2D Mater.*, vol. 3, p. 011005, feb 2016.
- [80] S. Haddad and L. Mandhour, “Kohn anomaly of optical zone boundary phonons in uniaxial strained graphene: Role of the Dirac cone electronic dispersion,” *Phys. Rev. B*, vol. 98, p. 115420, Sep 2018.
- [81] F. J. Peña and E. Muñoz, “Magnetostain-driven quantum engine on a graphene flake,” *Phys. Rev. E*, vol. 91, p. 052152, May 2015.
- [82] M. O. Goerbig, “Electronic properties of graphene in a strong magnetic field,” *Rev. Mod. Phys.*, vol. 83, pp. 1193–1243, Nov 2011.
- [83] M. O. Goerbig, J.-N. Fuchs, G. Montambaux, and F. Piéchon, “Tilted anisotropic Dirac cones in quinoid-type graphene and  $\alpha$ -(BEDT-TTF)<sub>2</sub>I<sub>3</sub>,” *Phys. Rev. B*, vol. 78, p. 045415, Jul 2008.
- [84] E. Lifshitz, A. M. Kosevich, and L. P. Pitaevskii, eds., *Theory of Elasticity*. Oxford: Butterworth-Heinemann, 3rd ed., 1986.

- [85] D. A. Papaconstantopoulos, M. J. Mehl, S. C. Erwin, and M. R. Pederson, “Tight-binding hamiltonians for carbon and silicon,” *MRS Proceedings*, vol. 491, p. 221, 1997.
- [86] Y. Concha, A. Huet, A. Raya, and D. Valenzuela, “Supersymmetric quantum electronic states in graphene under uniaxial strain,” *Mater. Res. Express*, vol. 5, p. 065607, jun 2018.
- [87] Ş. Kuru, J. Negro, and L. M. Nieto, “Exact analytic solutions for a Dirac electron moving in graphene under magnetic fields,” *J. Phys.: Condens. Matter*, vol. 21, p. 455305, oct 2009.
- [88] K. S. Novoselov, A. K. Geim, S. V. Morozov, D. Jiang, M. I. Katsnelson, I. V. Grigorieva, S. V. Dubonos, and A. A. Firsov, “Two-dimensional gas of massless Dirac fermions in graphene,” *Nature*, vol. 438, no. 7065, pp. 197–200, 2005.
- [89] Y. Zhang, Y.-W. Tan, H. L. Stormer, and P. Kim, “Experimental observation of the quantum Hall effect and Berry’s phase in graphene,” *Nature*, vol. 438, no. 7065, pp. 201–204, 2005.
- [90] G. Li and E. Y. Andrei, “Observation of Landau levels of Dirac fermions in graphite,” *Nat. Phys.*, vol. 3, no. 9, pp. 623–627, 2007.
- [91] I. Sahalianov, T. Radchenko, V. Tatarenko, and Y. Prylutsky, “Magnetic field-, strain-, and disorder-induced responses in an energy spectrum of graphene,” *Ann. Phys.*, vol. 398, pp. 80 – 93, 2018.
- [92] E. Díaz-Bautista and D. J. Fernández C., “Multiphoton supercoherent states,” *Eur. Phys. J. Plus*, vol. 134, p. 61, Feb 2019.
- [93] E. Díaz-Bautista, Y. Concha-Sánchez, and A. Raya, “Barut–Girardello coherent states for anisotropic 2D-Dirac materials,” *J. Phys.: Condens. Matter*, vol. 31, p. 435702, jul 2019.
- [94] E. Díaz-Bautista and D. J. Fernández, “Graphene coherent states,” *Eur. Phys. J. Plus*, vol. 132, p. 499, Nov 2017.
- [95] W. E. Lamb, “An operational interpretation of nonrelativistic quantum mechanics,” *Phys. Today*, vol. 22, no. 4, pp. 23–28, 1969.
- [96] K. Wódkiewicz, “Operational Approach to Phase-Space Measurements in Quantum Mechanics,” *Phys. Rev. Lett.*, vol. 52, pp. 1064–1067, Mar 1984.
- [97] A. Royer, “Measurement of the Wigner Function,” *Phys. Rev. Lett.*, vol. 55, pp. 2745–2748, Dec 1985.

- [98] D. T. Smithey, M. Beck, M. G. Raymer, and A. Faridani, “Measurement of the Wigner distribution and the density matrix of a light mode using optical homodyne tomography: Application to squeezed states and the vacuum,” *Phys. Rev. Lett.*, vol. 70, pp. 1244–1247, Mar 1993.
- [99] T. J. Dunn, I. A. Walmsley, and S. Mukamel, “Experimental Determination of the Quantum-Mechanical State of a Molecular Vibrational Mode Using Fluorescence Tomography,” *Phys. Rev. Lett.*, vol. 74, pp. 884–887, Feb 1995.
- [100] K. Banaszek and K. Wódkiewicz, “Direct Probing of Quantum Phase Space by Photon Counting,” *Phys. Rev. Lett.*, vol. 76, pp. 4344–4347, Jun 1996.
- [101] G. Breitenbach, S. Schiller, and J. Mlynek, “Measurement of the quantum states of squeezed light,” *Nature*, vol. 387, pp. 471–475, 1997.
- [102] K. Banaszek, C. Radzewicz, K. Wódkiewicz, and J. S. Krasinski, “Direct measurement of the Wigner function by photon counting,” *Phys. Rev. A*, vol. 60, pp. 674–677, Jul 1999.
- [103] P. Lougovski, E. Solano, Z. M. Zhang, H. Walther, H. Mack, and W. P. Schleich, “Fresnel Representation of the Wigner Function: An Operational Approach,” *Phys. Rev. Lett.*, vol. 91, p. 010401, Jun 2003.
- [104] H. J. Carmichael, *Statistical Methods in Quantum Optics 1. Theoretical and Mathematical Physics*, Springer-Verlag Berlin Heidelberg, 1999.
- [105] D. J. Callaway, “On the remarkable structure of the superconducting intermediate state,” *Nucl. Phys. B*, vol. 344, no. 3, pp. 627 – 645, 1990.
- [106] A. I. Zayed, *Handbook of function and generalized function transformations*. CRC Press, 1996.
- [107] Yuan, Y. and Li, K. and Wang, J. H. and Ma, K., “The Wigner Functions for a Spin-1/2 Relativistic Particle in the Presence of Magnetic Field,” *Int. J. Theor. Phys.*, vol. 49, pp. 1993–2001, Sep 2010.
- [108] C. Baune, J. Fiurášek, and R. Schnabel, “Negative Wigner function at telecommunication wavelength from homodyne detection,” *Phys. Rev. A*, vol. 95, p. 061802, Jun 2017.
- [109] A. Jalal and S. Iqbal, “Quantum Dynamical Behavior of the Morse Oscillator: the Wigner Function Approach,” *J. Russ. Laser Res.*, vol. 39, pp. 544–551, Nov 2018.
- [110] C. Zachos, “Deformation Quantization: Quantum Mechanics Lives and Works in Phase-Space,” *Int. J. Mod. Phys. A*, vol. 17, no. 03, pp. 297–316, 2002.
- [111] A. C. Hirshfeld and P. Henselder, “Deformation quantization in the teaching of quantum mechanics,” *Am. J. Phys.*, vol. 70, no. 5, pp. 537–547, 2002.